NRC Research Press

ARTICLE

Climate change and recent sedimentation in Nastapoka Sound, eastern coast of Hudson Bay

Maxime Jolivel, Michel Allard, and Guillaume St-Onge

Abstract: In an attempt to determine to what extent the impact of recent climate changes that occurred east of Hudson Bay, including important reduction of areas in permafrost, had on the coastal marine environment, a series of shallow cores were extracted from the seabed off the mouth of the Sheldrake River, in Nastapoka Sound. A total of 25 cores were taken in April 2009 from the ice cover. A preliminary seafloor map was first done to help in the selection of the coring sites. Nastapoka Sound has a complex subaqueous relief, formed of asymmetric ridges and deep basins. After preliminary sedimentological analyses, six of the cores were selected for physical and chronological analyses (^{14}C, ^{210}Pb, and ^{137}Cs dating); among them, three were selected for elemental (C, N, OC/TN) and isotopic (δ^{13}C, δ^{15}N) analyses to identify sedimentary organic matter sources. Sedimentation processes are complex and are primarily driven by bottom currents. This is confirmed by the absence of a clay fraction in several cores, some erosion surfaces in a few cores, and the presence of comet-like mark features on the seafloor. The highest sedimentation rates are found near the coast of the province of Quebec and Gillies Island and the lowest ones occur in the deep depocenters. Isotopic and elemental analyses reveal that Nastapoka Sound is an area of mixing between marine and terrestrial inputs and can be compared to an estuarine system similar to nearby Lac Guillaume-Delisle. Those conditions altogether make it difficult to extract a perfectly clear signal of climate change in the recent sediment record. However, the downcore application of a simple two end-member mixing model to measured δ^{13}C values strongly suggests that the fraction of sedimentary organic matter from terrestrial sources increased by 30% since about the middle of the Little Ice Age. This trend accelerated at the end of the 20th century. Rapid permafrost decay in adjacent river catchments is likely one source for this terrestrial carbon. However, it cannot be distinguished from other potential sources that are also related to environmental changes such as increase in primary productivity both on land, where peatlands, shrubs, and forest are expanding, and at sea, where sea ice cover duration is diminishing.

Résumé : Dans le but de déterminer l'étendue des impacts des changements climatiques récents qui ont eu lieu à l'est de la baie d'Hudson, incluant une réduction significative des secteurs de pergélisol, sur l'environnement marin côtier, une série de carottes peu profondes a été prélevée du lit marin à l'embouchure de la rivière Sheldrake, dans le détroit de Nastapoka. Un total de 25 carottes a été prélevé à partir de la couverture glaciaire en avril 2009. Une carte préliminaire du plancher océanique a été dressée afin d'aider à choisir les sites de prélèvement des carottes. Le détroit de Nastapoka a un relief subaquatique complexe, formé de crêtes asymétriques et de bassins profonds. Après des analyses sédimentologiques préliminaires, six carottes ont été choisies pour des analyses physiques et chronologiques (datation par ^{14}C, ^{210}Pb et ^{137}Cs); parmi celles-ci, trois ont finalement été sélectionnées pour des analyses élémentaires (C, N, C/N (carbone organique / azote total)) et isotopiques (δ^{13}C, δ^{15}N) afin d'identifier les sources de matières organiques sédimentaires. Les processus de sédimentation sont complexes et fortement influencés par les courants de fond. Cela est confirmé par l'absence d'une fraction argileuse dans plusieurs carottes, des surfaces d'érosion dans quelques carottes et la présence de marques de style comète sur le fond de l'océan. Les taux de sédimentation les plus élevés se trouvent à proximité de la côte de la province de Québec et de l'île Gillies et les taux les plus faibles se trouvent dans les endroits de déposition les plus profonds. Les analyses isotopiques et élémentaires montrent que le détroit de Nastapoka est un endroit de mélange entre les intrants marins et terrestres et qu'il peut être comparé à un système estuarien semblable à celui du Lac Guillaume-Delisle à proximité. Prises ensemble, ces conditions peuvent rendre difficile l'extraction d'un signe parfaitement clair de changement climatique dans le profil stratigraphique récent. Toutefois, l'application, au bas de la carotte, d'un modèle simple de mélange de deux extrémités, aux valeurs δ^{13}C mesurées suggère fortement que la fraction de matière organique sédimentaire provenant de sources terrestres s'est accrue de 30 % depuis environ le milieu du Petit Âge glaciaire. Cette tendance s'est accélérée à la fin du 20e siècle. Le déclin rapide du pergélisol dans des bassins hydrographiques adjacents constitue probablement une des sources de ce carbone terrestre. Toutefois, il ne peut pas être distingué d'autres sources potentielles qui sont aussi reliées à des changements environnementaux tels qu'une augmentation de productivité primaire à la fois sur terre, où s'étendent les tourbières, les arbustes et les forêts, et en mer où la durée de la couverture de glace diminue. [Traduit par la Rédaction]

Received 31 July 2014. Accepted 17 March 2015.

Paper handled by Associate Editor Olav Lian.

M. Jolivel and M. Allard. Centre d'études nordiques, Pavillon Abitibi-Price, 2405 de la Terrasse, Université Laval, Québec, QC G1V 0A6, Canada.
G. St-Onge. Institut des sciences de la mer de Rimouski and GEOTOP, Canada Research Chair in Marine Geology, Université du Québec à Rimouski, Rimouski, QC G5L 3A1, Canada.
Corresponding author: Maxime Jolivel (e-mail: maxime.jolivel.1@ulaval.ca).

Introduction

The Hudson Bay bottom sediments are of interest because they contain a record of the environmental changes that took place in the terrestrial environment of its surrounding catchment. Starting at the time of deglaciation, bottom morphology and sediments registered the catastrophic drainage of glacial Lake Agassiz-Ojibway into the North Atlantic (Lajeunesse and St-Onge 2008). Several other studies have focused on the glacial–postglacial transition of the Hudson Bay through analyses of sediment cores and seismostratigraphy (Bilodeau et al. 1990; Gonthier et al. 1993; Hill et al. 1999; Lavoie et al. 2008).

Many studies using sediment cores, mostly in coastal sectors of the bay, successfully yielded paleo-environmental reconstructions (Jenner and Piper 2002; Ladouceur 2008; Haberzettl et al. 2010). More recently, studies have focused on atmospheric and fluvial processes affecting modern sedimentation to better understand the sediment composition and sources (Hare et al. 2008; Kuzyk et al. 2008, 2009, 2010; Hülse and Bentley 2012). For instances, Kuzyk et al. (2008) showed evidences of temporal changes in the composition of terrigenous organic carbon (TOC) in Hudson Bay sediments and linked it to climate and the presence of ice. Another study conducted by Kuzyk et al. (2010) focused on the relative importance of marine versus terrestrial organic matter (TOM) inputs in Hudson Bay. Those studies, however, put the emphasis on spatial C distribution patterns in the surface sediment layer and did not document possible changes in the origin and accumulation rates of OM through time.

During the late Holocene and particularly in recent decades, the coastal region on the eastern side of Hudson Bay has experienced significant variations in air temperature, precipitation, and sea ice cover duration, which have affected environments by increasing their primary production and causing rapid permafrost thaw (Allard and Seguin 1987; Payette et al. 2004; Ladouceur 2008; Bhiry et al. 2011; Jolivel and Allard 2013). However, sedimentary studies attempting to decipher a marine record of geomorphological and ecological changes in the watershed are almost absent, one exception being research near the mouth of Rivière de la Grande Baleine reported by Hülse and Bentley (2012).

This study was conducted in Nastapoka Sound, offshore of a region where permafrost thaw and an increasing number of thermokarst features due to climate warming were reported over the late 20th Century (Marchildon 2007; Larouche 2010; Jolivel and Allard 2013). As the region was covered by vast expanses of frozen peatlands (palsa fields and plateaus) and by permafrost in fine-grained postglacial marine sediments, it could be expected that the extensive decay of permafrost could have been a source of OC and fine sediments that would have ended up being deposited in the marine environment, thus providing some record of climate-driven environmental change. A long-term increase in air temperature can also influence the transfer of TOM by a change of the hydrological regime of rivers, an acceleration of the erosion rates in the catchments, and an expansion of the shrub cover (e.g., Bowden et al. 2008; Myers-Smith et al. 2011). This concern is of great importance because these new inputs can alter aquatic ecosystems and affect food webs, especially in Subarctic and Arctic regions (Bowden et al. 2008).

The study period focused on the second half of the Little Ice Age (LIA) and the post-LIA time, i.e., the last 250 years. In the area, the LIA encompasses the colder period occurring between 1500 and 1850 AD (Allard and Seguin 1987; Haberzettl et al. 2010). Although precise dating is difficult to attain, evidence of warming has been observed through permafrost decay and increase in marine productivity since the end of the 19th century (Allard and Seguin 1987; Ladouceur 2008). The rate of thermokarst or permafrost decay got faster since about the mid-1990s in the region (Payette et al. 2004; Fortier and Aubé-Maurice 2008).

The objectives of this study are to detect and document possible changes in the supply of recent and modern sedimentary OM in the coastal Hudson Bay environment, particularly in relation to recent climate warming and permafrost decay. However, to achieve these goals it is necessary first to better understand the recent morpho-sedimentary dynamics through a characterization of the sedimentary environment, measurements of sediment accumulation rates, physical properties, and sedimentary structures on the seafloor of Nastapoka Sound. Presented are a number of different analyses and measurements to track changes over a 250 year period in a subarctic region very sensitive to climate change (Kerwin et al. 2004).

Setting

Hudson Bay is a fairly shallow inland sea that receives 30% of the total Canadian river flow over a catchment area of 3.1 million km^2 (Prinsenberg 1986; Kuzyk et al. 2008). Marine water inflows coming from the Arctic Ocean penetrate the bay via the northwest and leave it by the northeast through Hudson Strait, after having circulated in a counter-clockwise direction (Prinsenberg 1986).

The study area is located off the mouth of the Sheldrake River, on the eastern coast of the bay, in Nastapoka Sound (Fig. 1). This long and narrow (4–6 km), wide basin is located between the coast of Quebec and the Nastapoka Islands; it sits between two sets of late Proterozoic volcano-sedimentary cuestas that have steep cliffs facing east and gentle slopes plunging west under the sea. The series of islands is parallel to the circular arch of the bay from Le Goulet of Lac Guillaume-Delisle to Inukjuak170 km north. This semi-enclosed sedimentary basin played an important role during the Holocene by trapping glaciomarine, glaciofluvial, and postglacial marine sediments (Lavoie et al. 2008).

Following deglaciation, from 8200 cal. BP onward, the Tyrrell Sea inundated coastal areas, reaching up to 220 m above sea level (a.s.l.) at the head of the Sheldrake River basin (Lavoie et al. 2012). The postglacial emergence rate was 10 m per century immediately after deglaciation and then slowed. Today, it is 1.3 m per century (Allard and Seguin 1985; Lajeunesse and Allard 2003; Lajeunesse 2008; Lavoie et al. 2012).

Typically, three main marine sedimentary units reflect the glacial and postglacial history of the region (Bilodeau et al. 1990; Gonthier et al. 1993; Hill et al. 1999; Lavoie et al. 2002, 2008). Unit 1 is a subaqueous ice-contact and glaciomarine unit deposited by the melting ice sheet in contact with the Tyrrell Sea. Unit 2 is a paraglacial unit deposited during the transition between glaciomarine to modern conditions by the reworking and resedimentation of emerged glacial and glaciofluvial sediments. Unit 3 is a Late Holocene to modern unit associated with fluvio-deltaic and marine processes. At the scale of Hudson Bay, and depending on location, the Late Holocene unit is composed of sediments derived from erosion of glacigenic sediments (120×10^6 t/year), coastal erosion (18×10^6 t/year), fluvial inputs (10.2×10^6 t/year), and atmospheric deposition (0.74×10^6 t/year) (Hare et al. 2008). Sea-ice rafting is another source of sediment, but its input contribution is hard to quantify (Haberzettl et al. 2010). In Nastapoka Sound, acoustic profiles revealed a total sediment thickness of 10–30 m and a maximum of 70 m in deep troughs (Girard Thomas 2009; Lavoie et al. 2008). The seafloor morphology is very similar to the emerged topography with cuestas, glacial valleys, and east–west oriented troughs (Lavoie et al. 2008; Girard Thomas 2009).

On the floor of Nastapoka Sound, surface sediments are postglacial hemipelagic sediment deposited from suspension under a low-energy sedimentary regime (Lavoie et al. 2002; Lavoie et al. 2008; Girard Thomas 2009). Subaqueous topographic depressions, such as at the foot of Gillis Island, acted as traps for glacigenic, glaciomarine, and postglacial sediments, as shown by the greater thickness of the sedimentary deposits in these depocenters compared to more shallow areas (Girard Thomas 2009; Lavoie et al.

Fig. 1. Bathymetric map and location of the coring sites. Bathymetric data south of the unmapped areas come from Girard Thomas (2009).

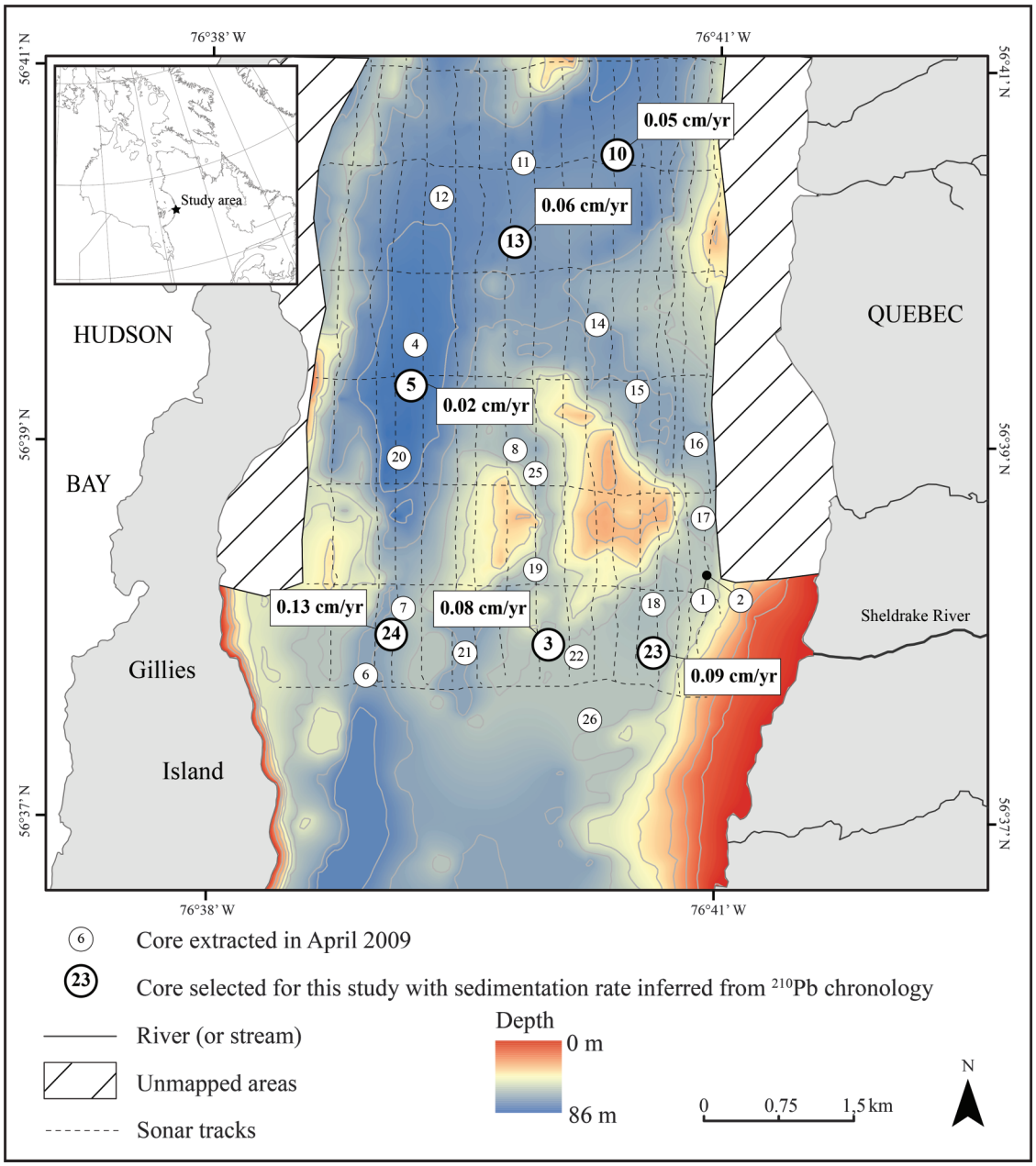

2008; Josenhans et al. 1988). Erosion by bottom currents locally leads to the outcropping of glaciomarine sediment on the seafloor. This was observed in Nastapoka Sound (Lavoie et al. 2008; Girard Thomas 2009), in Manitounouk Sound (Hill et al. 1999), and on most of the central Hudson Bay seafloor (Josenhans et al. 1988).

In Nastapoka Sound, strong surface currents flow from south to north at velocities reaching 15–20 cm/s (Saucier et al. 2004). Bottom currents are slower and can be reversed southward (Saucier et al. 2004), but their dynamics still remain largely undocumented. The mean tidal range is approximately 1 m (Lavoie et al. 2002).

The area experiences a subarctic climate with cold winters (daily average temperature of –24 °C in January) and cool summers (daily average temperature of 10 °C in July). As a result, Nastapoka Sound, similarly to almost the whole Hudson Bay, is totally frozen from mid-December to mid-June. However, recent global warming induces a later freeze-up and an earlier break-up (Gagnon and Gough 2005).

In the region, the most important rivers flowing into the bay are the Nastapoka River (30 km north of the study area), the Little Whale River (70 km south), and the Great Whale River (170 km south) with an average yearly discharge of 7.86, 3.74, and 19.77 km^3/yr, respectively (Déry et al. 2005). The 780 km^2 estuary of Lac Guillaume-Delisle receives fresh water from four principal rivers and connects with Hudson Bay by a narrow and shallow channel named Le Goulet, 50 km south of the study area. The annual discharge of this freshwater system is 4.49 km/yr (Déry et al. 2005). According to Déry and Wood (2004), large-scale climatic teleconnections, such as the Arctic Oscillations, are the main factors influencing the variability and trend of Canadian high-latitude freshwater discharge.

The Sheldrake River drains a catchment covered by discontinuous permafrost that has been widely impacted by thermokarst for many decades (Jolivel and Allard 2013). In that river catchment,

Table 1. Features of the 25 sediment cores extracted in April 2009.

Core	Longitude	Latitude	Depth (m)	Core length (cm)	Sediment texture	Sedimentary structures	IRD
1	76°33′5″W	56°38′13″N	52	7	Coarse sand	No	Yes
2	76°33′5″W	56°38′13″N	52	12	Coarse sand	No	Yes
3	76°34′35″W	56°37′49″N	70	39	Very coarse silt to very fine sand	No	Yes
4	76°36′0″W	56°39′25″N	80	34	Massive silt (a) and sand (b)	Change in sedimentation from fine (a) to coarse (b) upcore (10 cm)	Yes
5	76°36′1″W	56°39′13″N	82	39	Coarse silt to fine sand	An erosion contact (10 cm) separates convolutes (downcore) and stratified sediment (upcore)	Yes
6	76°36′25″W	56°37′37″N	71	31	Massive silt (a) and sand (b)	Sand bed (11 cm); convolutes (b) (19 cm downcore); change in sedimentation from fine (a) to coarse (b) (11 cm)	Yes
7	76°36′2″W	56°37′59″N	62	36	Massive silt (a) and sand (b)	Probable erosion contact (15 cm) associated with a change in sedimentation from fine (a) to coarse (b) upcore	Yes
8	76°34′59″W	56°38′52″N	65	27	Silty sand	Three sand beds (10, 16, 22 cm)	Yes
10	76°34′0″W	56°40′29″N	73	33	Coarse silt to fine sand	Two erosion contacts (20 and 28 cm)	Yes
11	76°35′0″W	56°40′24″N	74	31	Silt	No	Yes
12	76°35′47″W	56°40′13″N	77	30	Silt	No	Yes
13	76°35′1″W	56°40′0″N	72	38	Very coarse silt	No	No
14	76°34′12″W	56°39′33″N	69	25	Silt	No	Yes
15	76°33′48″W	56°39′12″N	68	15	Silt	Erosion contact (5 cm) with truncated convolutes	Yes
16	76°33′12″W	56°38′54″N	68	19	Silt, sand, and gravel	No	Yes
17	76°33′6″W	56°38′31″N	64	15	Silt, sand, and gravel	No	Yes
18	76°33′36″W	56°38′3″N	62	11	Silt and sand	No	Yes
19	76°34′45″W	56°38′13″N	65	34	Massive silt (a) and sand (b)	Change in sedimentation from fine (a) to coarse (b) (13 cm)	Yes
20	76°36′9″W	56°38′47″N	82	38	Massive silt (a) and sand (b)	Change in sedimentation from fine (a) to coarse (b) (23 cm)	Yes
21	76°35′26″W	56°37′46″N	70	31	Silt	Sand bed (18 cm)	Yes
22	76°34′23″W	56°37′47″N	63	20	Silt and sand	No	Yes
23	76°33′33″W	56°37′48″N	61	27	Coarse silt to fine sand	No	No
24	76°36′12″W	56°37′52″N	64	26	Coarse silt to medium sand	Three sand beds (10, 14, 20 cm)	Yes
25	76°34′46″W	56°38′44″N	65	40	Massive silt (a) and sand and gravel (b)	Probable erosion contact (7 cm) with change in sedimentation from fine (a) to very coarse (b) upcore	Yes
26	76°34′12″W	56°37′24″N	60	27	Silt and sand	Contact erosion (7 cm); sand bed (22 cm)	Yes

Note: Sediment textures and structures are given from visual inspection and CT-scan imagery, except cores 3, 5, 10, 13, 23, and 24 (grain size analyses). IRD is ice-rafted debris. (a) and (b) in sedimentary structures referred to the given (a) and (b) sediment texture.

the total permafrost area was reduced by 21% between 1957 and 2009, thus potentially providing a significant release of sediments and C through the fluvial system (Jolivel and Allard 2013). It was estimated that this small river exported 160 t of sediments in 2010 and 117 t of sediments in 2013. Thermokarst and periglacial processes are responsible for periods of turbidity in mid-summer. For example, over 24 days in 2010 and 19 days in 2013, starting around 10 July, 53% and 25%, respectively, of the total annual suspended sediment load was delivered to the sea through the Sheldrake River (Jolivel 2014).

Methods

Marine geophysical surveys

Bathymetric surveys were performed in July 2008 from the MV Katherine-Anne with a Raymarine DSM300 digital sounder module (200 kHz) connected to a Raymarine C80 series display with NMEA output and coupled with an Edgetech 4100P sidescan sonar (100 kHz). Sixteen longitudinal and seven latitudinal track lines were surveyed. Distance between two longitudinal lines was ~250 m and distance between two latitudinal lines was ~400 m. The goal was to map seabed morphology and to localize areas that are likely to be efficient sediment traps for recent deposition from rivers. The mapping starts at a distance ~1.5 km parallel to the low lying coast of the Province of Quebec until ~200 m from the steep shores of Gillies Island. The map was realized with the ArcGis software by ordinary kriging, with 2028 selected depth points. Sidescan images were visualized using Discover 4100 software. South of 56°38′, bathymetric data from Girard Thomas (2009) were used to complete the map. The bathymetric data from Girard Thomas were digitized from PDF files. Girard Thomas (2009) used a Knudsen 320 B/P sonar (200 kHz) coupled with a GPS. Map matching was done with ArcGis software.

The coring sites were selected from the bathymetric map and seafloor images in sectors susceptible to be covered by soft sediments. Twenty-five short sediment cores were extracted from the ice cover in April 2009 with a K-B gravity corer (16 kg). The valve mechanism allowed for minimal frontal wave effect and the water–bottom interface was well preserved in the sampling process. Cores were 20–40 cm long and were recovered in depths between 52 and 82 m. Sediment cores were stored at 4 °C until their analyses in the laboratory. For this study, after a visual analysis of all the cores (Table 1), six were selected according to their location (cores 03, 05, 10, 13, 23, and 24): they are all located in the deeper areas and along a transect off the mouth of the Sheldrake River (Fig. 1).

Table 2. ^{14}C ages.

Core	Sediment depth (cm)	Sample description	^{14}C age (±)	Age cal. BP (years) (2σ range) Lower limit	Upper limit	Mean	Laboratory No.
23a	14	Unidentified shell fragments	1845 (15)	1123	1304	1210	ULA-1593
24	21.5	Unidentified shell fragments	2320 (15)	1605	1847	1730	ULA-1589
23b	16	Unidentified shell fragments	2350 (15)	1639	1875	1760	ULA-1591
03a	20.5	Bulk sediment	2650 (20)	1995	2278	2140	ULA-1764
03b	30	Bulk sediment	6165 (20)	6287	6502	6390	ULA-1765

Laboratory methods

All cores were first analyzed through CT-Scan (Institut National de la Recherche Scientifique, Eau, Terre, Environnement, Quebec City) with 1 mm resolution to visualize sedimentary structures, shells, and ice-rafted debris (Orsi et al. 1994). CT-scanning also allows for imaging of density contrast showed by gray scale values expressed in CT-numbers (e.g., St-Onge and Long 2009). CT-numbers can give indications of changes in density, mineralogy, and OM content (e.g., Crémer et al. 2002; St-Onge et al. 2007; St-Onge and Long 2009; Fortin et al. 2013). The cores were then split and run for magnetic susceptibility (k) at 0.5 cm intervals using a GEOTEK multi-sensor core logger at the Institut des sciences de la mer de Rimouski.

Grain size analysis were performed at 1 or 2 cm interval for each of the six cores. Carbonates and OM were removed using HCl acid and loss-on-ignition treatments. To exclude ice-rafted material, the fine fraction was separated from the coarse fraction with a 500 μm sieve. Only the finest fraction was kept and analyzed with a Horiba laser sizer, after disaggregation in an ultrasonic bath. The results of at least three runs were averaged. Grain size parameters were calculated using Gradistat 8.0 software (Blott and Pye 2001). Mean grain sizes are used for interpretation and discussion.

Dating

^{210}Pb and ^{137}Cs analyses were performed at the radiochronology laboratory of Université Laval by gamma ray counting. Recent sedimentation rates were estimated from profiles of radioactive decay of ^{210}Pb in association with the nuclear fallout of ^{137}Cs. Subsamples were extracted downcore at 1 cm intervals. The "constant flux-constant sedimentation" model used here allowed estimation of sedimentation rates in centimetres per year according to the slope of the ln-linear regression of $^{210}Pb_{in\ excess}$ activity with depth. The constant flux/constant sedimentation model assumes that the initial flux of ^{210}Pb in the system and the derived sedimentation rate are constant through time (e.g., O'Reilly et al. 2010).

The low level of ^{210}Pb and ^{137}Cs activity, close to detector background in some samples (especially in cores 05, 23, and 24), is a potential source of uncertainty. The activity of $^{210}Pb_{in\ excess}$ was measured graphically from the radioactive decay ^{210}Pb profiles. The slope is calculated from the ln $^{210}Pb_{in\ excess}$ versus depth graph. Analytical uncertainties have been calculated on the trend line of the time-depth profiles with a confidence interval of 95%.

Deeper samples in cores 13, 23, and 24 contained traces of ^{137}Cs, thus preventing the use of first entry of ^{137}Cs in 1953 (date of first input of this radioisotope in the environment). Therefore, as is usually done (Klaminder et al. 2012), sedimentation rates from ^{137}Cs were calculated from the 1963 (year of fallout maximum) peak concentration as follows:

$$(1) \qquad S = (C_{max} - L_b)/(T - 1963)$$

where S is sediment accumulation rate (cm/yr), C_{max} the maximum concentration depth (cm) of ^{137}Cs, L_b the mixing layer thickness, and T the year of sample collection.

In addition, three shell fragments and two bulk clay samples containing OM were submitted to AMS (Accelerator Mass Spectrometry) ^{14}C dating. The ^{14}C ages were calibrated using CALIB 6.1 software (Stuiver and Reimer 1993). A ΔR value of 180 ± 40 years was used for the marine reservoir effect correction (Barber et al. 1999; McNeely et al. 2006; Lavoie et al. 2012). Calibrated ages presented in the text are the mean ages between the upper and lower limits of the calibrated radiocarbon range. The calibrated ages ranges themselves are given in Table 2.

Sedimentation rates from ^{210}Pb profiles were extrapolated until 1750, i.e., in the second half of the LIA. In this study, the dating exceeds the maximum depth of $^{210}Pb_{in\ excess}$, implying uncertainties. However, when sediments are homogenous in density and grain size, as in this study, it is commonly deemed acceptable date sequences up to 250 years (e.g., Liu et al. 2007).

C, N, δ^{13}C, and δ^{15}N analysis

C, N, δ^{13}C, and δ^{15}N analysis were performed at the G.G. Hatch Isotope Laboratories, University of Ottawa, on cores 03, 13, and 23. Each sample was divided into three subsamples. The first subsample was treated twice with 10% HCl acid to remove carbonates and then washed three times (dried and milled). This subsample was used to determine total C (TC) and total N (TN) with a Carlo-Erba elemental analyser. The second subsample was used to determine residual N and C, which is considered to represent OC, and to analyse for δ^{13}C. The third one was used for δ^{15}N. The second and third subsamples were previously dried, milled, and sieved. OC/TN weight ratio was converted into the molar ratio by multiplying by 14/12 (Lamb et al. 2006).

As determined by routine replicate measurements of standards in the analytical laboratories, analytical precision of OC and TN contents is ±0.02% and ±0.01%, respectively; it is ±0.04‰ and ±0.4‰ for δ^{13}C and δ^{15}N isotope measurements, respectively.

Historical changes in the fraction of terrestrial organic matter

To estimate the historical changes in the fraction of TOM in marine sediment of the Nastapoka Sound, a two end-member mixing model proposed by Calder and Parker (1968) was applied

$$(2) \qquad \%TOM = (\delta^{13}C_{marine} - \delta^{13}C_{observed})/(\delta^{13}C_{marine} - \delta^{13}C_{terrigenous}) \times 100$$

where $\delta^{13}C_{marine}$ and $\delta^{13}C_{terrigenous}$ are the marine and the terrestrial end-member values for Hudson Bay, respectively (Kuzyk et al. 2010), i.e., –20.8‰ and –28.2‰; and $\delta^{13}C_{observed}$ is the measured δ^{13}C of a given sample.

Results

Seafloor morphology and distribution of surface sediments

Sidescan images and direct observation of cores revealed a complex surface sediment distribution. In general, fine sediments are located in the deepest areas or basins, while coarser material is

Fig. 2. Erosional landforms on the seafloor. (A) comet-like mark features (encircled); (B) erosion channel (arrow).

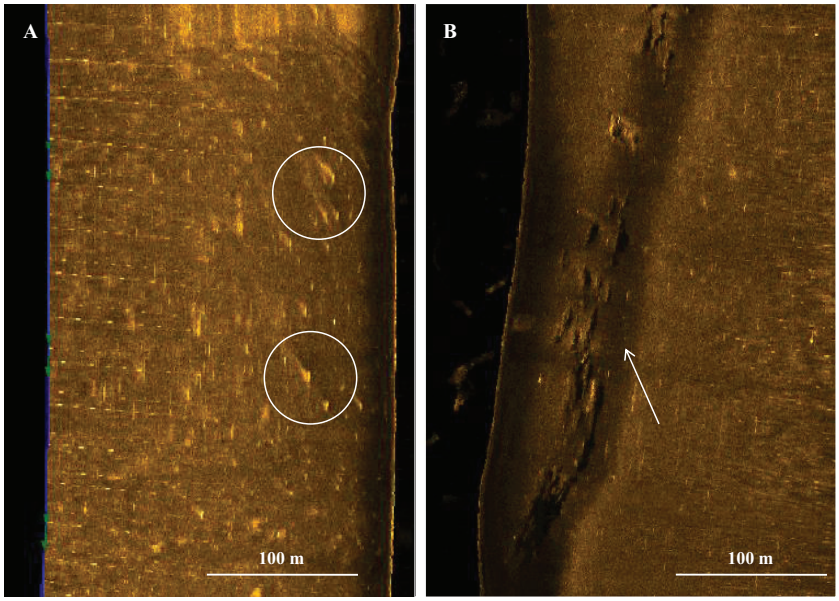

concentrated near the coast, near Gillies Island, and at the bottom of the slopes of submarine hills. Ice-rafted gravel and sand are dispersed over the seafloor. Bedrock outcrops appear as knobs. The bathymetric data acquired do not allow for a precise description of the subaqueous relief and the sediment distribution in the shallow nearshore zone. However, at very low tide, mud deposition can be observed on the flats near the mouth of the Sheldrake River.

The two asymmetric east–west ridges (low cuestas ridges) in the center of the area are characteristic of the continental and marine regional landscapes. The range in elevation between the top and the foot of the escarpment of the two ridges is ~40 m, while the dip slope extends over 1000–2500 m. The deepest areas are situated along Gillies Island and in the northern part of the studied area. Depth reaches 85 m at the foot of the escarpment edge of the cuesta forming Gillies Island. Side-scan imagery shows the presence of comet-like features and erosion channels at the base of ridge escarpments (Fig. 2).

Chronology

^{210}Pb and ^{137}Cs data and profiles are shown in Fig. 3. According to profiles of $^{210}Pb_{in\ excess}$, sedimentation rates vary between 0.02 ± 0.01 and 0.13 ±0.04 cm/year. The lowest accumulation rates occurred in the deepest central basin (0.02 ±0.01 and 0.06 ± 0.02 cm/year). The highest sedimentation rates are recorded near the coast (0.09 ± 0.03 cm/year) and near Gillies Island (0.13 ± 0.04 cm/year). A thin surface mixing layer is present in cores 10, 23, and 24. The data from these zones were not used for establishing chronology by excess ^{210}Pb. The depth of supported ^{210}Pb was not reached in core 24. We used the deepest point as the supported ^{210}Pb. Consequently, the sedimentation rate inferred for core 24 should be considered as a minimum.

Five samples from various depths in three different cores were submitted for radiocarbon dating. Shells yielded ages of 1210 (1123–1304) cal.^{14}C BP, 1730 (1605–1847) cal.^{14}C BP, and 1760 (1639–1875) cal.^{14}C BP, while the bulk C samples yielded ages of 2140 (1995–2278) cal.^{14}C BP and 6390 (6287–6502) cal.^{14}C BP (Table 2).

Lithology and grain size

In the six cores, sediments are visually similar (Figs. 4 and 5). They consist of compact medium silt to medium sand with rare shell fragments, traces of bioturbation, some black reduction spots, and scattered drop sand and gravel. Mean grain size ranges from 27 to 64 μm. A clay fraction is absent or negligible. The grain-size distributions are generally bimodal and very-poorly sorted (Fig. 6). The most prominent mode at 5 μm corresponds to the fine silt fraction, and the second mode at ~40 μm corresponds to coarse silt to fine sand. Three erosional contacts are recorded in cores 05 and 10. They are revealed by truncated beds on CT-scan images and by changes in the CT-number, mean grain size and *k* value.

Core 05 shows soft sediment deformations from ~12 cm downward (Fig. 4). Convolutes, in the form of sand waves and wavy and nonparallel stratifications, are observed on the CT-scan image and by variations in *k* and CT-number. In cores 13, 24, and 05, mean grain size tends to increase toward the sediment surface, while cores 03, 10, and 23 show no significant trend grain size variation.

Elemental and isotopic composition of sedimentary organic matter

Sediments have very low TN and OC contents of ≤ 0.15% and ≤ 0.8%, respectively (Table 3). In general, values are constant or increase slightly toward the surface, except TN in core 23 which shows an opposite pattern. C/N molar ratios vary between 1 and 11. δ^{13}C values range from –23.3‰ to –25.1‰, while δ^{15}N values range from 6.5‰ to 9.2‰. Cores 03, 13, and 23 registered a general decrease in δ^{13}C and δ^{15}N toward the surface, except for core 03 which does not show a significant vertical trend in δ^{15}N (Table 3). Core 23 registered a clear steady increase in C/N molar ratio toward the surface, whereas the C/N of core 03 shows no particular trend; in core 13, it tends to decrease toward the surface. On the other hand, in all cores, the surface layer (2–3 cm thick) is marked by a more pronounced increase in C/N while δ^{13}C and δ^{15}N decrease (Table 3; Fig. 5).

Discussion

Sedimentation rates and chronology

Radiocarbon ages of the three shell fragments collected from cores 23 and 24 yielded calculated sedimentation rates of ~0.01 cm/year (Table 2). No erosion surfaces are visible in these cores. ^{210}Pb chronology shows sedimentation rates of 0.09 ± 0.03 (core 23) and 0.13 ± 0.04 cm/year (core 24). Sedimentation rates off Le Goulet at the outlet of the Lac Guillaume-Delisle (Haberzettl et al. 2010), as well as those off the mouth of the Great Whale River, are similar to those derived by the ^{210}Pb chronology of this study (Jenner and Piper 2002; Kuzyk et al. 2008; Hülse and Bentley

Fig. 3. ^{210}Pb activity profiles (total and in excess) (closed diamonds) and ^{137}Cs (open squares) concentration. Shaded zones indicate the surface mixed layer. The dashed lines illustrate the supported ^{210}Pb. SAR is sediment accumulation rate.

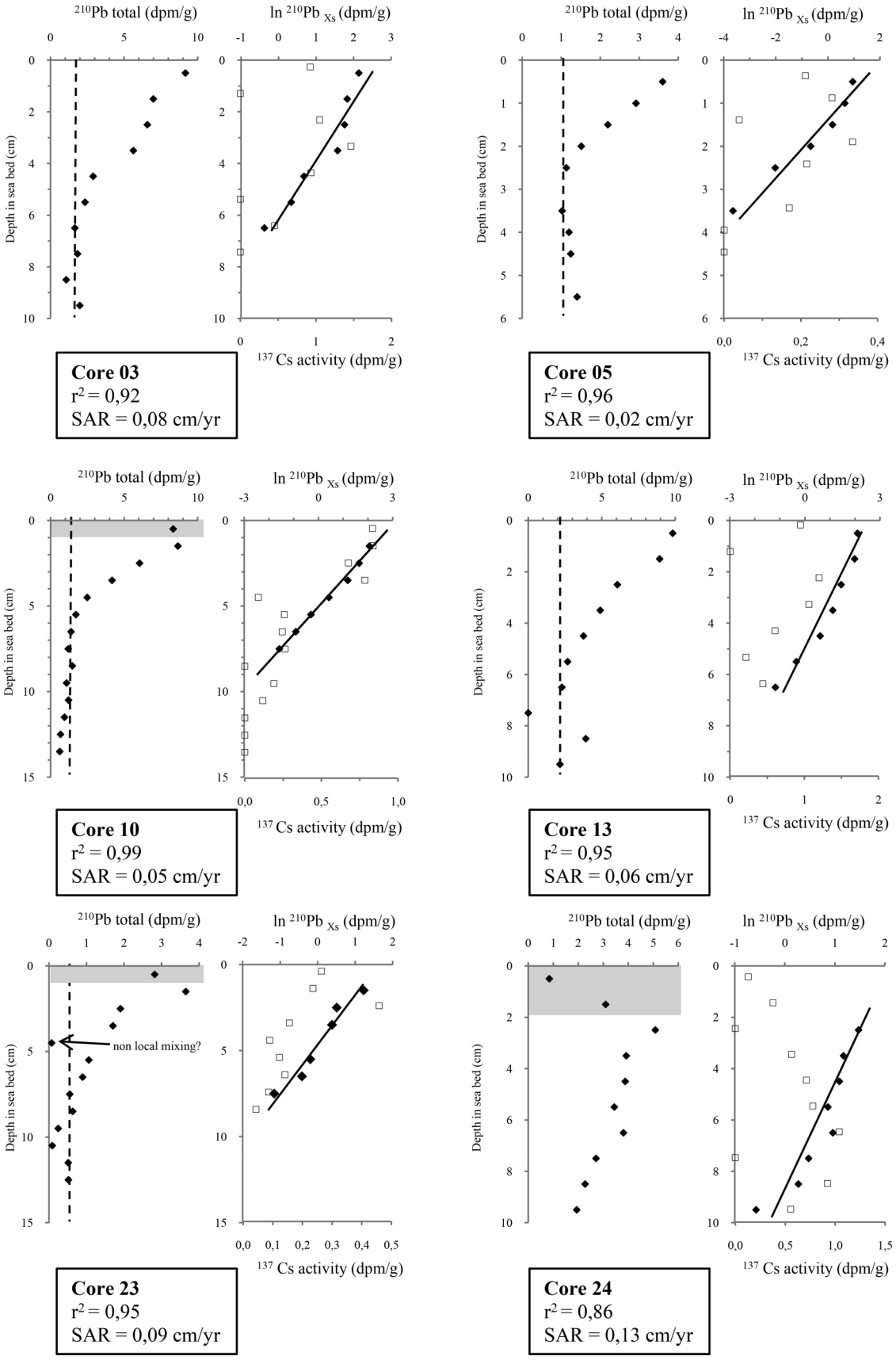

Fig. 4. CT-scan image, mean grain size (μm), magnetic susceptibility (*k*), and CT-number of cores 05, 10, and 24. A zoom of the CT-scan image in core 05 highlights the convolutes and the erosional contact. Light gray bands show erosional contacts in cores 05 and 10; darker gray bands highlight sand beds in core 24. The closed star indicates 1900 AD inferred from ^{210}Pb profiles.

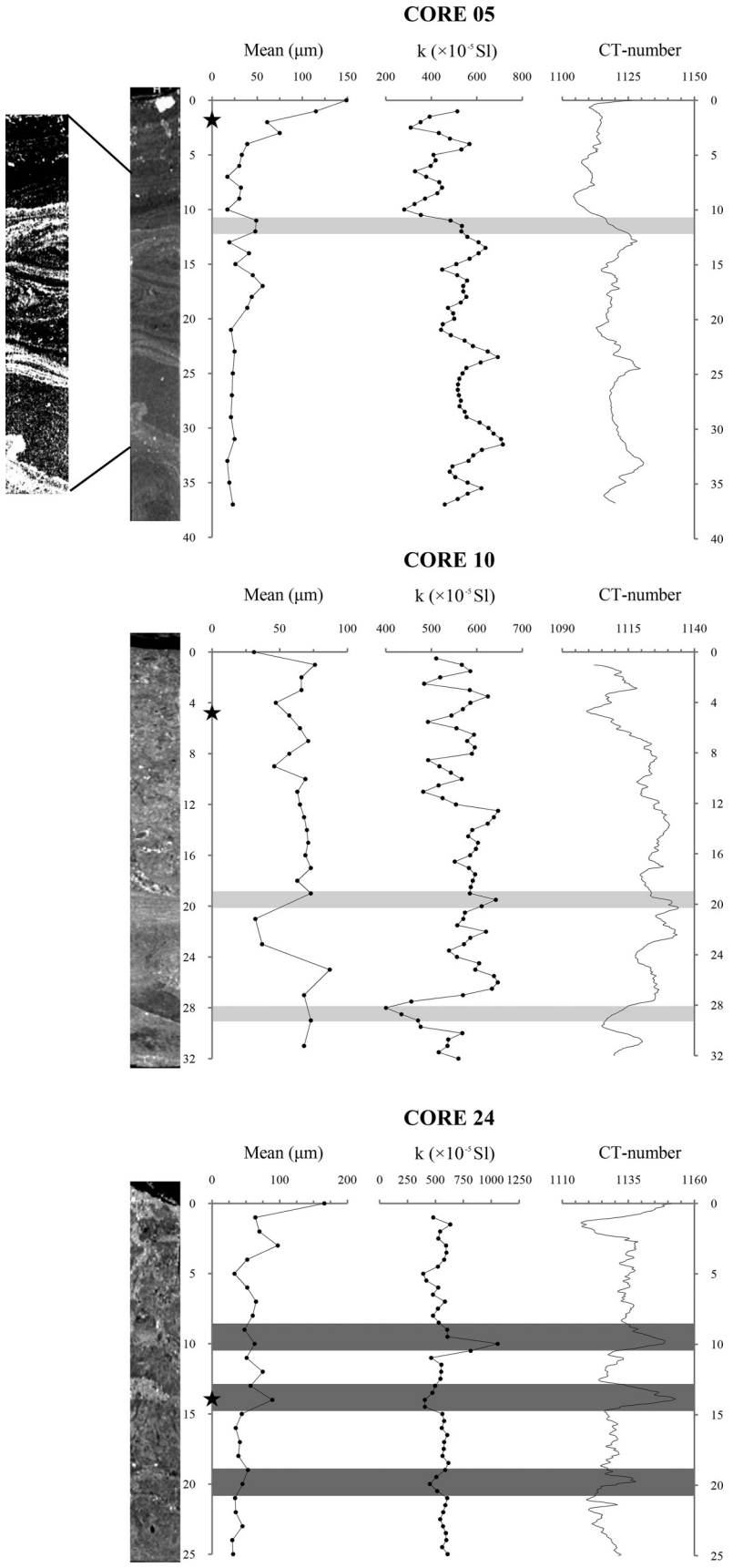

Fig. 5. CT-scan images, physical, elemental, and isotopic composition profiles of cores 03, 13, and 23. The closed star indicates 1900 AD inferred from ^{210}Pb profiles.

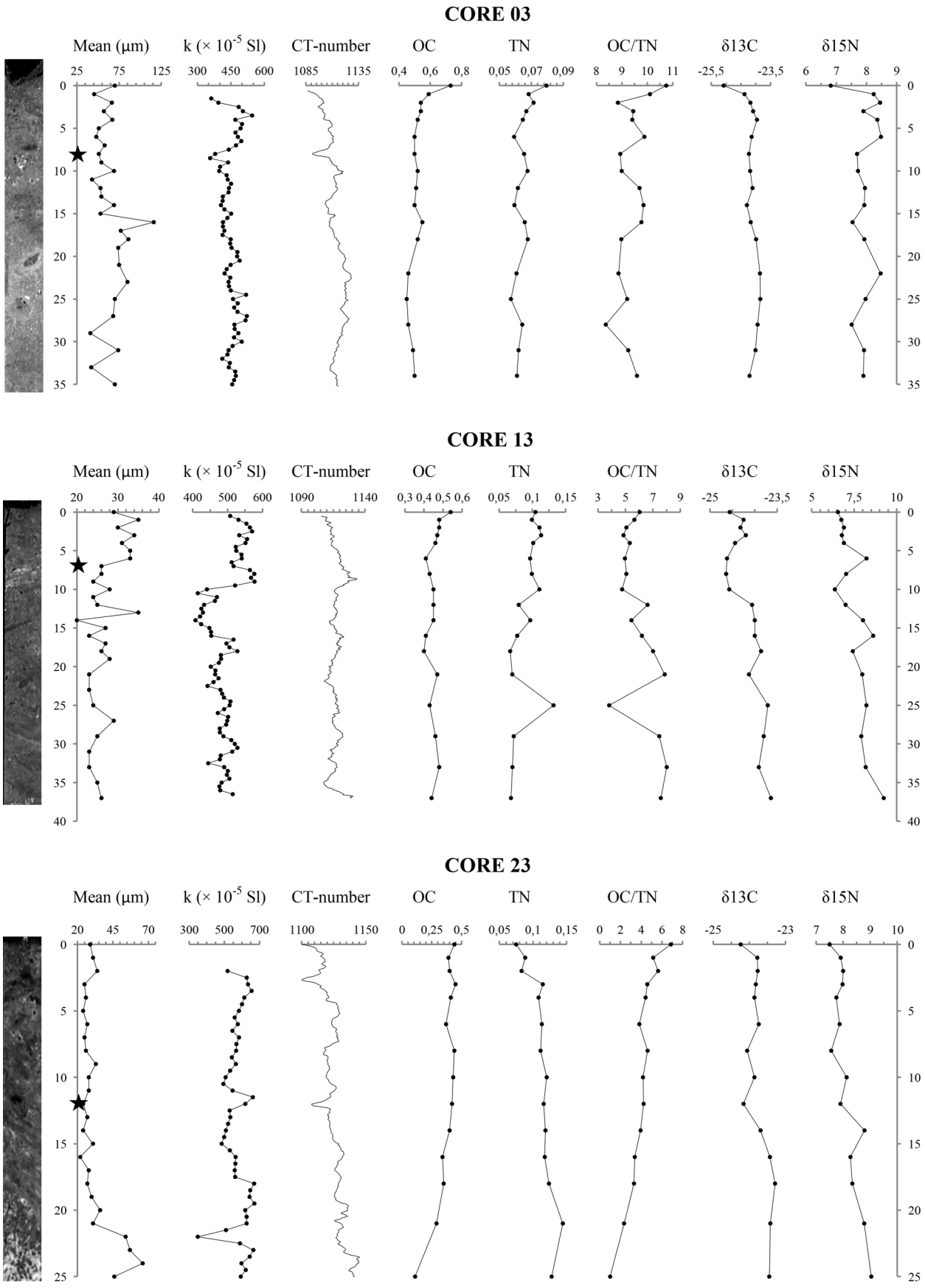

Fig. 6. Average grain size distribution for core 13. Note the bimodal distribution.

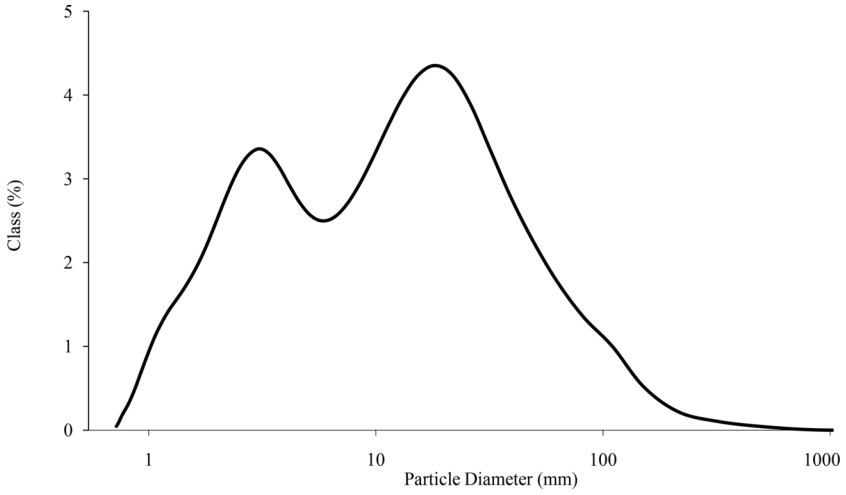

2012). Therefore, it is likely that the three shell fragments provide inexact ages either because they have been redeposited or because the marine C reservoir (ΔR) was underestimated.

As for shell dating, the radiocarbon ages on bulk C appear considerably older than expected with the ^{210}Pb chronology and when compared to ages obtained in other studies in the region. It is thus likely that recycled older C was introduced in the sedimentary system. Similarly, older C is also observed in bottom sediments of thermokarst lakes near Kuujjuarrapik (Bouchard et al. 2012). Indeed, numerous peatlands affected by thermokarst, riverbank, and coastal erosion are a potential source of old C in the coastal marine environment (Guo et al. 2004).

For the six cores, ln $^{210}Pb_{in\ excess}$ profiles are well established (Fig. 3) despite the presence of a thin surface mixing layer in cores 23 and 24. This linear pattern reflects constant sedimentation rates, as observed off the Great Whale River mouth (Hülse and Bentley 2012). The preservation of a bioturbation overprint confirms slow sediment accretion rates that allowed for biological activity (Bentley et al. 2006). Low sedimentation rates also imply large time intervals per centimetre of accumulation (1 cm = 8 to 50 years of sedimentation). This may explain the bimodal and the very-poorly sorted grain size distribution as subsampling at 1 cm intervals cannot reflect intra-interval environmental changes, and shorter-term variations in sedimentary regimes.

The ^{210}Pb profiles are validated by the ^{137}Cs measurements. Indeed, for cores 03, 13, and 24, the depth of maximum concentration of ^{137}Cs confirmed the ^{210}Pb chronology. On the other hand, the ^{137}Cs maximum concentration is deeper than expected with the ^{210}Pb chronology in cores 10 and 23 (and to a lesser extent in core 24). This can possibly be linked to the downward diffusion of ^{137}Cs as a result of surface sediment mixing (Robbins et al. 1978) and (or) of diffusion in pore water (Klaminder et al. 2012). On the contrary, in core 05, the ^{137}Cs maximum concentration is shallower than expected. The presence of ^{137}Cs near the surface sediment and the relative low amplitude of the peak of ^{137}Cs can be associated with a deferred supply of ^{137}Cs occurring when freshwater sediments are transferred to the marine environment (Oughton et al. 1997; Klaminder et al. 2012). This process may be enhanced by remobilization of emerged sediments in a context of isostatic rebound. Finally, the 1 cm resolution subsampling and the low sedimentation rate imply a non-negligible margin of error about the maximum concentration depth of ^{137}Cs.

The mean local sediment accumulation rate (0.07 cm/year) is in accordance with the only other available radiocarbon dated chronology in the area, 0.09 cm/year in the outlet of Lac Guillaume-Delisle (Haberzettl et al. 2010). However, it is slightly lower than in central and western Hudson Bay despite the fact that eastern Hudson Bay receives sediment inputs from large rivers, such as the Great Whale River and the Innuksuac River (Jenner and Piper 2002; Kuzyk et al. 2008, 2009; Hülse and Bentley 2012). Our new sedimentation rates in Nastapoka Sound support the interpretation that this basin is an energetic environment affected by strong currents (Saucier et al. 2004) and that sediment inputs from rivers of the southeastern Hudson Bay are either deposited in the proximal river mouth area or dispersed in a northward direction in the counter-clockwise current circulation and in the Hudson Bay system in general (Hülse and Bentley 2012).

In the studied area, sedimentation rates range from 0.02 ± 0.01 to 0.13 ± 0.04 cm/year depending on location. Deep basins generally registered lower sedimentation rates than shallow coastal sites. However, there is no relationship between sediment accretion rates and water depth, distance from the coast, or distance from the Sheldrake River mouth, as observed off the Great Whale River (Hülse and Bentley 2012). This confirms that deposition processes are primary driven by local marine hydrodynamics and are not significantly affected by rivers located 70 km (the Little Whale River) and 170 km (the Great Whale River) to the south. In the proximal area, rivers have low discharge; for instances, Sheldrake River has a mean annual discharge of only 17 m^3/s (Jolivel 2014). Consequently, fluvial sediment inputs are not sufficient to offset reworking of sediments by marine processes.

A complex sedimentary regime

In the studied area, several lithological features and bottom landforms reflect the influence of bottom currents. This influence is shown by the quasi-absence of clay in every core, erosion contacts in cores 05 and 10, the presence of comet-like mark features and erosional channels (Fig. 2), and possible current megaripples on the seafloor (Girard Thomas 2009). The uneven subaqueous relief seems to influence bottom currents, which increase in velocity along topographic sills and are channelled into erosional scours (Girard Thomas 2009; Fig. 2).

In core 05, reworked sediments, in the form of convolutes, are evidenced in stratified sediments, with black OM rich beds (Fig. 4). Truncated stratification reveals an erosion contact at ~12 cm deep. The very low sedimentation rates in the upper part of the core and the thin recent sediment layer (only 12 cm thick) exclude the hypothesis that the convolutes are recent load structures.

This kind of convolute is likely made by gravity flows and liquefaction of soft sediments (Lajeunesse and Allard 2002). The only seismic unit showing evidence of gravity flow, hummocky deposits, and disturbed sediment deposits in the Nastapoka and Manitounouk sounds is a rapid basin infilling unit deposited during

Table 3. Downcore analytical results for elemental and isotopic data from cores 03, 13, and 23.

Depth (cm)	OC (%)	N (%)	C/N	$\delta^{13}C$ (‰)	$\delta^{15}N$ (‰)
Core 03					
0	0.73	0.08	10.75	−25.08	6.82
1	0.59	0.07	10.11	−24.38	8.24
2	0.54	0.07	8.84	−24.18	8.45
3	0.54	0.07 (0.07)	9.45	−24.09	7.90 (8.12)
4	0.52	0.06	9.41	−23.96	8.36
6	0.5	0.06	9.89	−24.14	8.48
8	0.5 (0.5)	0.07	8.94	−24.21 (−24.23)	7.69
10	0.52	0.07	9.00	−24.19	7.72
12	0.51	0.06	9.70	−24.11	7.95
14	0.5	0.06	9.85	−24.30	7.93
16	0.55	0.07	9.77	−24.17	7.54
18	0.52	0.07	8.98	−23.99	7.93
22	0.46	0.06	8.87	−23.86	8.47
25	0.45	0.06	9.21	−23.85	7.97
28	0.46	0.06 (0.06)	8.37	−23.94	7.51 (7.72)
31	0.49	0.06	9.25	−24.01	7.92
34	0.5 (0.49)	0.06	9.60	−24.21 (−24.13)	7.90
Core 13					
0	0.54	0.10	6.04	−24.56	6.55
1	0.48	0.10	5.65	−24.25	6.75
2	0.48	0.11	5.07	−24.32	6.90
3	0.47	0.11	4.86	−24.20	6.78
4	0.46	0.10	5.32	−24.44	6.90
6	0.41	0.10	4.96	−24.62	8.23
8	0.43	0.10 (0.10)	5.07	−24.64	7.03 (6.20)
10	0.45	0.11	4.76	−24.57	6.37
12	0.45	0.08	6.61	−24.06	7.00
14	0.45	0.10	5.44	−24.00	8.02
16	0.41	0.08	6.20	−24.00	8.62
18	0.4 (0.39)	0.07	7.01	−23.86 (−23.95)	7.42
21	0.47	0.07	7.86	−24.13	7.98
25	0.43	0.13	3.82	−23.71	8.22
29	0.46	0.07	7.47	−23.80	7.92
33	0.48	0.07	8.01	−23.91	8.18
37	0.44	0.07 (0.07)	7.58	−23.64	9.24 (9.34)
Core 23					
0	0.44	0.07	6.87	−24.24	7.50
1	0.39	0.09	5.16	−23.78	7.91
2	0.4 (0.39)	0.08	5.64	−23.77 (−23.85)	8.00
3	0.45	0.11	4.59	−23.82	7.98
4	0.41	0.11	4.43	−23.86	7.75
6	0.37	0.11	3.82	−23.74	7.87
8	0.44	0.11	4.62	−24.06	7.56
10	0.43	0.12	4.18	−23.86	8.13
12	0.42	0.12	4.24	−24.16	7.90
14	0.4	0.12	3.95	−23.69	8.79
16	0.34*	0.12	3.38	−23.43	8.27*
18	0.35*	0.12 (0.15)	3.31	−23.29	8.34 (9.19)*
21	0.29 (0.34)*	0.14	2.35	−23.42 (−23.29)	8.78*
25	0.11*	0.13	1.01	−23.45	9.04*

Note: Data in brackets are quality control duplicates.

*Indicates low to very low N amount, as a consequence, N and $\delta^{15}N$ values must be considered with particular caution.

the transition between glaciomarine and marine conditions (Hill et al. 1999; Lavoie et al. 2008; Girard Thomas 2009). The location of the coring site in a deep depocenter and the fact that this unit can be affected by erosion (Lavoie et al. 2002) would support the hypothesis that the disturbed sediment observed in core 05 belongs to this seismic unit.

The thin layer that caps the sequences suggests a rather recent change in the bottom currents and the sedimentary regime, from erosion or no deposition to depositional conditions. This transition would have occurred by ~1400 AD based on the sedimentation rate derived at core 05 with ^{210}Pb data (0.02 ± 0.01 cm/year). Contemporary marine conditions have generally existed since 6500 yr. BP, i.e., since the end of the glaciomarine phase (Bilodeau et al. 1990). Continuous fall of the relative sea level has likely influenced the water circulation and sediment transport in the sound, as a result of the progressive closure of Manitounouk Sound further south (Allard and Tremblay 1983). Since the side-scan imagery does not reveal any specific surface landforms at the coring site, it is likely that the area has experimented a recent change in the dynamic of the bottom currents.

The CT-scan image of core 24 reveals sand beds characterised by an increase in mean grain size and CT-number and a decrease or increase in *k* (Fig. 4). CT-number seems to indicate an inverse-to-normal grading typical of hyperpycnal flow caused by periods of high discharge (Mulder et al. 2003). However, this trend was not recorded in any other cores located near or in front of the Sheldrake river mouth (Table 1). First entry of ^{137}Cs is deeper in the sequence than the upper-most sand bed, and no erosion contact is visible, suggesting that the upper sand beds are recent (~1940 AD for the upper one).

The bathymetric map (Fig. 1) shows that core 24 was extracted at the foot of a steep slope, on an elevation of the seafloor between two deeper basins. These narrow corridors between two topographic obstacles are favourable to increased bottom current velocity (Hill et al. 1999; Girard Thomas 2009). This core registered the highest sedimentation rate of the area, suggesting that bottom current deposits or (and) contourite deposits (Girard Thomas 2009) are a significant source of sediment in this particular area.

Four other cores, which were not physically analysed, have visible sand beds on CT-scan imagery (Table 1). Three of them (cores 6, 8, and 21) are located in the same topographic environment, i.e., in submarine valleys or corridors (Fig. 1). Thus, sand beds may be originated by recurrent periods of highest energy allowing transport of larger particles. According to that interpretation, the gradually upward increasing mean grain size, also observed in cores 05 and 13 (Figs. 4 and 5), could be related to a recent increase in energetic marine conditions in Nastapoka Sound, as proposed by Hülse and Bentley (2012) for Manitounouk Sound.

Origin of recent sedimentation

$\delta^{13}C$ and C/N

$\delta^{13}C$ and C/N are efficient tracers for TOM in Hudson Bay (Kuzyk et al. 2010) because they provide an estimate of the relative proportions of marine and terrestrial sources of OM in marine sediments (e.g., Naidu et al. 1993; Meyers 1994; Thornton and McManus 1994; St-Onge and Hillaire-Marcel 2001; Lamb et al. 2006). $\delta^{13}C$ and C/N in surface sediment both decrease with increasing water depth, latitude, and distance from the coast in Hudson Bay (Kuzyk et al. 2010), in the St. Lawrence Estuary and Gulf (Muzuka and Hillaire-Marcel 1999), and in the Arctic Ocean (e.g., Naidu et al. 2000; Nagel et al. 2009). This is due to the progressive mixture of terrestrial and marine OM along a gradient of distance to shore.

The isotopic signature of OM is preserved in sediments through long periods of time, even if OM may continue to be degraded (Meyers 1994). However, decomposition of OM during transport, deposition, and diagenesis can be a source of biochemical alteration of isotopic and elemental C properties (e.g., Thornton and McManus 1994; Meyers 1997; Lamb et al. 2006). In this study, sedimentary facies are homogenous and similar. Moreover, no evidence of diagenesis, i.e., C/N and $\delta^{13}C$ are not correlated with sedimentation rates (Kuzyk et al. 2010), and no significant change of mean grain size that could biases $\delta^{13}C$ and C/N molar ratios (Gearing et al. 1977; Meyers 1994; Thornton and McManus 1994; Meyers 1997) were found in the vertical sequences. This absence of diagenetic effects in Hudson Bay surface sediment was also reported by Kuzyk et al. (2010). However, the low contents of N (≤0.15%) and OC (≤0.8%) can be a source of uncertainties (Sampei and

Fig. 7. $\delta^{13}C$ versus C/N in the surface sediments of the Nastapoka Sound (open squares) compared with values from Lac Guillaume-Delisle (closed triangles) and in the rest of Hudson Bay (closed circles). The oval highlights the similar isotopic composition of Nastapoka Sound sediments to estuarine sediments of Lac Guillaume-Delisle.

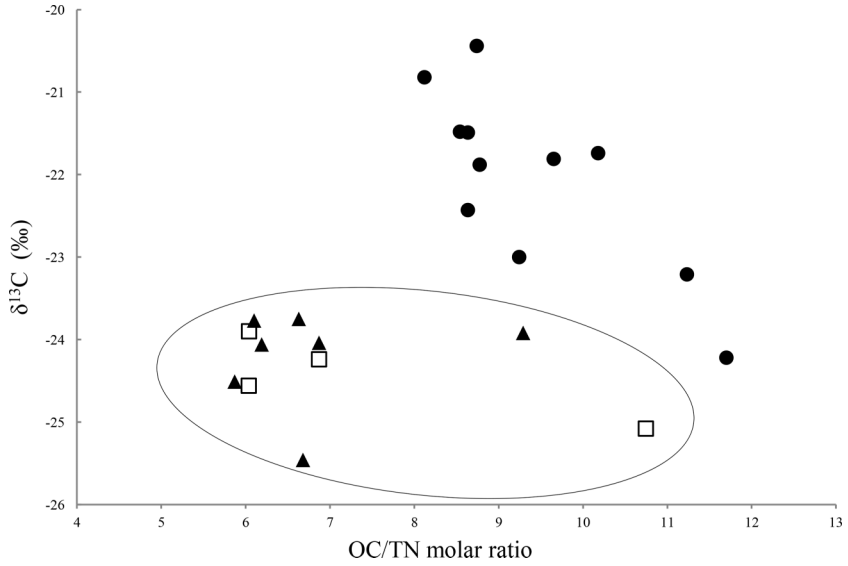

Matsumoto 2001; Lamb et al. 2006; Lavoie et al. 2008) and do not allow for interpretations of downcore changes.

$\delta^{13}C$ and C/N molar ratio in the surface sediments of the Nastapoka Sound (Fig. 7) show an influence of both marine productivity and terrestrial C3 plants (e.g., Lamb et al. 2006), as shown by Kuzyk et al. (2010) for the entire Hudson Bay. Moreover, $\delta^{13}C$ versus C/N molar ratio in Nastapoka Sound are distinctive from the rest of Hudson Bay (>25 km offshore) but similar to values found in Lac Guillaume-Delisle (Fig. 7). This indicates that Nastapoka Sound is an area that undergoes a significant terrestrial influence, i.e., similar to the estuarine conditions of Lac Guillaume-Delisle. Nastapoka Islands likely act as a barrier by holding freshwater and nutrient inputs released by numerous rivers flowing into James Bay and eastern Hudson Bay (Hudon et al. 1996; Déry et al. 2005). Moreover, the counter-clockwise water circulation and strong coastal currents may limit offshore dispersion of river inputs. Finally, although it is situated in the deepest area, core 03 recorded the highest recent terrestrial signal, indicating that deep depocenters are efficient traps for terrigenous sediment.

$\delta^{15}N$

In correlation with C/N molar ratio and $\delta^{13}C$, $\delta^{15}N$ of sedimentary OM also may provide an estimate of contributions of marine and terrestrial sources (e.g., Naidu et al, 2000; St-Onge and Hillaire-Marcel 2001; Nagel et al. 2009). $\delta^{15}N$ tends to decrease away from the coastline (e.g., Guo et al. 2004; Gaye et al. 2007; Nagel et al. 2009). In Hudson Bay surface sediments, there is a general spatial correspondence of $\delta^{15}N$ with C/N and $\delta^{13}C$: highest $\delta^{15}N$ values are found in the central and western Hudson Bay and lower values are recorded in the south and eastern Hudson Bay, showing a more relative terrestrial influence in the south of the Bay (Kuzyk et al. 2010). Our study confirms this trend: $\delta^{15}N$ of surface sediments in the Nastapoka Sound is similar to values found in southern and eastern coastal Hudson Bay and lower than in sediments of the central Hudson Bay.

$\delta^{15}N$ is sometimes used as an isotope signal from permafrost soils (Nagel et al. 2009). Indeed, low values of $\delta^{15}N$ may indicate colder climate with tundra vegetation or a catchment where permafrost was more abundant than today (Voss et al. 2006; Nagel et al. 2009). Additionally, OM released from permafrost catchments is less degraded than in permafrost free catchments and $\delta^{15}N$ stays low (Guo et al. 2004; Nagel et al. 2009). A general decrease of $\delta^{15}N$, as observed in cores 13 and 23, could suggest an increase of permafrost thickness and spatial distribution and a rarefaction of vegetation cover, associated with colder conditions. However, recent changes in landscapes around southeastern Hudson Bay registered the opposite trend (e.g., Payette et al. 2004; Bhiry et al. 2011).

This study indicates that the sedimentary OM of the Nastapoka Sound comes from a mixture of terrestrial and marine sources. However, the absence of correlation (not shown) between $\delta^{15}N$ and $\delta^{13}C$ and between $\delta^{15}N$ and C/N reveals that $\delta^{15}N$ is not only influenced by the relative mixing of the marine and terrigenous sources. The increase of $\delta^{15}N$ toward the surface in cores 13 and 23 also indicates that permafrost decay on nearby land since the LIA had no significant impact on N in OM released in the Nastapoka Sound. These findings support the idea that river inputs are a relatively low source of N compared to upwelling of deep water in coastal regions of Hudson Bay (Kuzyk et al. 2010). $\delta^{15}N$ in surface sediment is mostly influenced by the variability of the $\delta^{15}N$ of the phytoplankton in surface water and post-production processes (Kuzyk et al. 2010). Consequently, $\delta^{15}N$ appears as an inadequate proxy for studying changes in the OM sources in Nastapoka Sound and as an indicator of changes in permafrost extent over land.

Historical changes in the proportion of TOM since the LIA

Using eq. (2) and extrapolated sediment rates, the historical proportion of TOM since the second part of the LIA (~ 1750 AD) is represented for cores 03, 13, and 23 (Fig. 8). Available records of annual air temperatures and annual liquid precipitations going back to 1926 in Kuujjuarapik are also presented for comparison. A 5-years running average was applied to smooth the curves to match somewhat the smoothing effect created by the 1 cm thick $\delta^{13}C$ subsampling along the cores.

In the three cores, minimum of TOM, reflected by two subsamples in each cores, are recorded at the end of the LIA, in the early 19th century. During the LIA, terrain conditions were drier than today, which supposes lower river discharge, and so less TOM input in Hudson Bay. Those drier conditions were reflected by the low water level of lakes as a result of snow deficit until ~1750 AD and a higher frequency of forest fires in northern Quebec (Payette and Filion 1993; Payette et al. 2008). Also during LIA, the permafrost was aggrading in the region (Allard and Seguin

Fig. 8. Variation in the proportion of terrestrial organic matter (TOM) in cores 03, 13, and 23 since 1750 AD. Arrows highlight common trends. Coefficient of correlation between TOM curves are core 3/core 13: 0.7; core 3/core 23: 0.5; core 13/core 23: 0.8. Mean annual air temperature and mean liquid precipitation between 1926 and 2009 with 5-year running mean (dark line) of the Kuujjuarapik weather station which is located 125 km south of the study site.

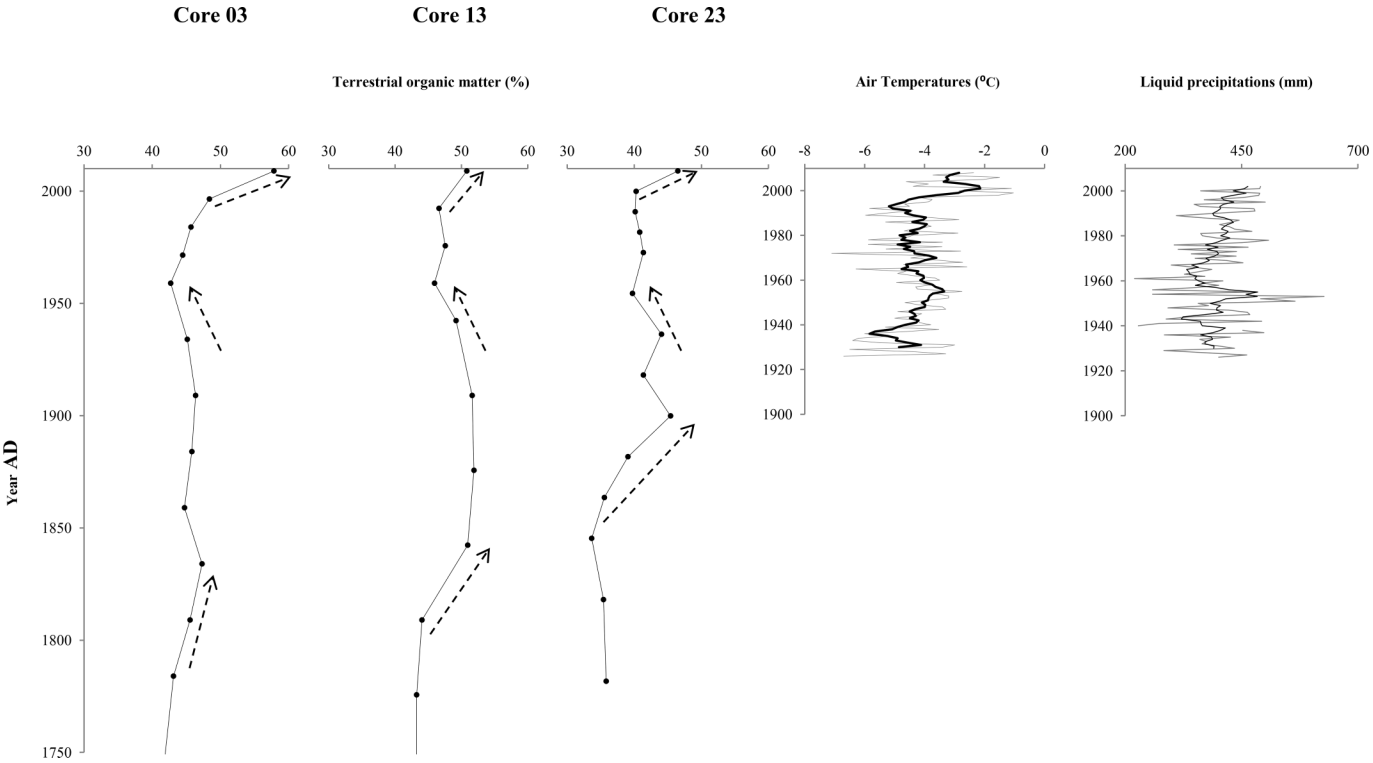

1987) limiting thermokarst which can be a significant source of terrigenous inputs in fluvial systems (Jolivel and Allard 2013).

The terrigenous fraction increased from the first part of the 19th century (cores 03 and 13) and from 1850 AD (core 23). In core 13, this pattern coincides with an increase in mean grain size and *k* and a decrease in the CT-number. Since ~1850 AD, mean annual air temperatures, precipitations, and river water level gradually increased in northern Quebec (Payette and Delwaide 1991, 2000), which likely resulted in a rise of fluvial inputs into Hudson Bay. This period of higher discharge corresponds with low $\delta^{13}C$ in coastal surface sediment (Gaye et al. 2007). The permafrost also started to decay at the end of the 19th century (Payette and Delwaide 2000) and, as a result, thermokarst activity must have increased. Permafrost thawing was then continuous during the 20th century (Payette et al. 2004). A significant rise in summer surface water temperature and salinity and a decrease in the duration of the ice cover, leading to an increase of marine productivity, were also observed at the end of the 19th century (Ladouceur 2008). This trend does not clearly appear in the TOM proportion neither in the indicators of production (OC, TN), but it may be reflected by an increase in $\delta^{15}N$ in the three cores around 1900 (Figs. 5 and 8). Finally, in her high resolution study that spans the period 1830–1992, Ladouceur (2008) measured a considerable increase of autotroph dynokist, and a decrease in heterotroph dynokist during that period. This would indicate a change of the type of productivity from a marine-dominated type (heterotroph dynokists) to a freshwater-dominated one (autotroph dynokists) concomitant with a reduction in the duration of sea ice cover (Ladouceur 2008).

The three cores revealed a decrease of TOM proportion in 1940–1950 AD with a minimum reached around 1960 AD. The time interval associated each with a 1 cm sample corresponds to 11–17 years. Because of this poor time resolution, these minimums likely reflect a multi-year trend. Unfortunately, no discharge data are available in the region for this period. However, the end of the 1950s and the 1960s correspond to a worldwide decrease in air temperature (Jones et al. 1999) and more specifically to a decrease in liquid and solid precipitations in the region (Payette and Delwaide 1991; Payette et al. 2004) (Fig. 8). A thinner snow pack would have resulted in lower melt water during snowmelt, reducing the intensity of the spring freshet during which much of sediment and nutrient are exported into Hudson Bay (Hudon et al. 1996).

The three cores registered an important increase of TOM influence in recent decades. This increasing trend is likely a response of the recent increase in air temperature recorded in north-eastern Canada since the early 1990s (Chouinard et al. 2007; Fig. 8), correlated with a general increase in liquid precipitation (Fig. 8) and river discharge (Déry et al. 2009). This recent trend is also confirmed by the decrease in $\delta^{15}N$ and the rise in C/N in the first centimetres toward the surface of each core. The recent climate change possibly affects the proportion of TOM in the surface sediment of the Nastapoka Sound in a couple of different ways. First, the rate of permafrost decay has increased considerably since the beginning of the 1990s (Payette et al. 2004). The core closest to the Sheldrake River mouth (core 23) shows the most obvious trend of an increasing TOM influence, i.e., the decrease of $\delta^{13}C$ is supported by a continuous increase in C/N and a decrease in $\delta^{15}N$ (Fig. 5). The constant mean grain size of core 23 suggests no change in Sheldrake River discharge and the increase of TOM proportion could be interpreted as a local signal of change in the river catchment where permafrost decay is very active. Second, the accelerated rate of erosion of peatlands and palsas since the early 1990s can also be an important source of TOM in that coastal area (Brown et al. 2003).

Over the last four decades, Hudson Bay sea ice began to form later and break-up earlier, particularly along the southern shore (Gagnon and Gough 2005), losing an average of 11.3% of its summer sea ice cover per decade (Tivy et al. 2011). This lengthening of the ice free period favours more energetic marine conditions and

offshore transport of terrestrial matter (Hülse and Bentley 2012). Due to the Hudson Bay's counter-clockwise circulation, it is likely that a part of the TOM released by large rivers south of the area (Great Whale River, Little Whale River) disperses along the eastern coast of Hudson Bay (Hülse and Bentley 2012) and reaches our study area. In this context, it is possible that an increasing volume of this material settles in Nastapoka Sound, even if no evidence is observed in mean grain size and in sedimentation rates. Later freeze-up and earlier break-up also imply that coastal areas are less protected from erosion by waves, especially during fall storms. Thus, coastal erosion could also potentially be a source of TOC that can contribute to lower $\delta^{13}C$ in the marine environment (Rachold et al. 2000). However, the coastline of the bay and the islands in the region is dominated by rocky ledges and gravel beaches. Therefore, fluvial inputs from rivers draining catchments affected by decaying peat-rich permafrost, by other erosional processes and by other wetland processes are the most probable sources for the recent increase in TOM. For instance, a lignin study by Kuzyk et al. (2008) revealed that sedimentary TOM in southern Hudson Bay is composed from a mixture of angiosperm and gymnosperm and woody and nonwoody plant material. This material is thought to come from several sources such as erosion of peat deposits, soil erosion along river banks, erosion of organic soils, and old marine and fluvial sediments originally from the Tyrrell Sea.

Finally, development of soils and vegetation in this zone of transition can be another factor leading to an increase of terrestrial inputs. This trend has already been showed following the last deglaciation (Miltner et al. 2005; Lavoie et al. 2008). Recent climate change has contributed to an increase of the shrub cover (Myers-Smith et al. 2011), particularly in coastal areas of Hudson Bay since the early 20th century (Laliberté and Payette 2008). This is likely to increase the influence of C3 plants on OM composition released by rivers, lowering its $\delta^{13}C$. However, these changes seem too recent to be recorded in marine sediments. Moreover, modern plants debris is thought to be retained near river mouth as a result of hydrodynamic sorting (Kuzyk et al. 2008).

The fraction of TOM in the surface sediment of the Nastapoka Sound has been found to vary through time since the LIA. The proportion of terrigenous versus marine OM has increased by 30% (core 03: +41%; core 13: +19%; core 23: +28%) over that period. It is now ≥50% in the surface sediments of Nastapoka Sound, which is higher than in offshore areas (≥25 km from the coastline) of southeastern Hudson Bay, where it varies between 15% and 35% (Kuzyk et al. 2010). The same general trend appears in the three cores with more or less amplitude and precision (Fig. 8).

Conclusion

Nastapoka Sound is an energetic marine environment. Subaqueous topography is complex and favours strong bottom currents, which control processes of sedimentation and erosion, as shown by comet-like mark sedimentary structures and erosional channels on the seafloor. Low sedimentation rates, erosional surfaces, changes in sediment texture, and the absence of clay in the cores also reflect this influence. Our study has shown that the velocity and the direction of bottom currents varied through time, likely in response to change in hydrodynamics.

Despite these strong marine hydrodynamics, the surface sediments of Nastapoka Sound recorded recent changes in the source of the OM. Nastapoka Sound is an area of mixture between marine and terrestrial inputs and can be compared to an estuarine system. The downcore study of OM origin reveals that TOM input is now higher that marine OM. Since the end of the LIA, contribution of TOM to marine sedimentation has increased by 30%. Despite some chronological uncertainties, it is clear that coastal eastern Hudson Bay has experienced noticeable changes in sediment inputs and origin since the LIA. The evolution of the terrestrial ecosystems affected by permafrost decay likely took part in the observed marine changes.

Acknowledgements

This project was supported by grants from ArcticNet and the Natural Science and Engineering Research Council of Canada (discovery grants to M.A. and G.St-O.). The Centre d'études nordiques of Université Laval provided important logistical support. Authors sincerely thank Bill Doidge for his personal availability, the use of his boat (the MV Katherine-Anne), and its equipment. Thanks are due to Emmanuel L'Hérault, Maud Audet Morin, and Carl Barrette for help in mapping; and Donald Cayer, Valérie Mathon Dufour, and Catherine Falardeau-Marcoux for assistance with grain size analyses. Jacques Labrie (Institut des sciences de la mer de Rimouski) is thanked for his help during the multi-sensor core logger measurements. Comments by Mickael Lemay on an earlier version of the manuscript are appreciatively acknowledged. The authors are also grateful to the Inuit community of Umiujaq for its generous hospitality and support on the ice, particularly to Joshua Sala and Peter Novalinga. Finally, P. Lajeunesse (Université Laval), D. Fortier (Université de Montréal), Ali Polat, Olav B. Lian, and two anonymous reviewers are thanked for their useful comments.

References

Allard, M., and Seguin, M.K. 1985. La déglaciation d'une partie du versant hudsonien québécois: bassins des rivières Nastapoka, Sheldrake et à l'Eau Claire. Géographie Physique et Quaternaire, **39**: 13–24. doi:10.7202/032581ar. [In French.]

Allard, M., and Seguin, M.K. 1987. The Holocene evolution of permafrost near the tree line, on the eastern coast of Hudson Bay (northern Quebec). Canadian Journal of Earth Sciences, **24**(11): 2206–2222. doi:10.1139/e87-209.

Allard, M., and Tremblay, G. 1983. La dynamique littorale des îles Manitounuk durant l'Holocène. Zeitschrift für Geomorphologie, Suppl. **47**: 61–95. [In French.]

Barber, D.C., Dyke, A., Hillaire-Marcel, C., Jennings, A.E., Andrews, J.T., Kerwin, M.W., et al. 1999. Forcing of the cold event of 8,200 years ago by catastrophic drainage of Laurentide lakes. Nature, **400**: 344–348. doi:10.1038/22504.

Bentley, S.J., Sheremet, A., and Jaeger, J.M. 2006. Event sedimentation, bioturbation, and preserved sedimentary fabric: field and model comparisons in three contrasting marine settings. Continental Shelf Research, **26**: 2108–2124. doi:10.1016/j.csr.2006.07.003.

Bhiry, N., Delwaide, A., Allard, M., Bégin, Y., Filion, L., Lavoie, M., et al. 2011. Environmental change in the Great Whale River region, Hudson Bay: five decades of multidisciplinary research by Centre d'études nordiques (CEN). Ecoscience, **18**: 182–203. doi:10.2980/18-3-3469.

Bilodeau, G., de Vernal, A., Hillaire-Marcel, C., and Josenhans, H.W. 1990. Postglacial paleoceanography of Hudson Bay: stratigraphic, microfaunal, and palynological evidence. Canadian Journal of Earth Sciences, **27**(7): 946–963. doi:10.1139/e90-098.

Blott, S.J., and Pye, K. 2001. GRADISTAT: a grain size distribution and statistics package for the analysis of unconsolidated sediments. Earth Surface Processes and Landforms, **26**: 1237–1248. doi:10.1002/esp.261.

Bouchard, F., Pienitz, R., Ortiz, J.D., Francus, P., and Laurion, I. 2012. Palaeolimnological conditions inferred from fossil diatom assemblages and derivative spectral properties of sediments in thermokarst ponds of subarctic Quebec, Canada. Boreas, **10**: 575–595. doi:10.1111/bor.12000.

Bowden, W.B., Gooseff, M.N., Balser, A., Green, A., Peterson, B.J., and Bradford, J. 2008. Sediment and nutrient delivery from thermokarst features in the foothills of the North Slope, Alaska: Potential impacts on headwater stream ecosystems. Journal of Geophysical Research, **113**: G02026. doi:10.1029/2007JG000470.

Brown, J., Jorgenson, M.T., Smith, O.P., and Lee, W. 2003. Long-term rates of coastal erosion and carbon input, Elson Lagoon, Barrow, Alaska. *In* Eighth International Conference on Permafrost, 21–25 July 2003, Zurich, Switzerland. Balkema Publishers, Zurich. pp. 101–106.

Calder, J.A., and Parker, P.L. 1968. Stable carbon isotope ratios as indexes of petrochemical pollution of aquatic systems. Environmental Science and Technology, **2**: 535–539. doi:10.1021/es60019a001.

Chouinard, C., Fortier, R., and Mareschal, J.-C. 2007. Recent climate variations in the subarctic inferred from three borehole temperature profiles in northern Quebec, Canada. Earth and Planetary Science Letters, **263**: 355–369. doi:10.1016/j.epsl.2007.09.017.

Crémer, J.-F., Long, B., Desrosiers, G., and De, Montety, L. 2002. Application de la scanographie à l'étude de la densité des sédiments et à la caractérisation des structures sédimentaires : exemple des sédiments déposés dans la rivière Saguenay (Québec, Canada) après la crue de juillet 1996. Canadian Geotechnical Journal, **39**(2): 440–450. doi:10.1139/t01-101. [In French.].

Déry, S.J., and Wood, E.F. 2004. Teleconnection between the Arctic Oscillation and Hudson Bay river discharge. Geophysical Research Letters, **31**: L18205. doi:10.1029/2004GL020729.

Déry, S.J., Stieglitz, M., McKenna, E.C., and Wood, E.F. 2005. Characteristics and trends of river discharge into Hudson, James, and Ungava Bays, 1964–2000. Journal of Climate, **18**: 2540–2557. doi:10.1175/JCLI3440.1.

Déry, S.J., Hernandez-Henriquez, M.A., Burford, J.E., and Wood, E.F. 2009. Observational evidence of an intensifying hydrological cycle in northern Canada. Geophysical Research Letters, **36**: L13402. doi:10.1029/2009GL038852.

Fortier, R., and Aubé-Maurice, B. 2008. Fast permafrost degradation near Umiujaq in Nunavik (Canada) since 1957 assessed from time-lapse aerial and satellite photographs. *In* Proceedings of the 9th International Conference on Permafrost, 28 June - 3 July 2008, Fairbanks, Alaska. Institute of Northern Engineering, University of Alaska, Fairbanks, AK. Vol. 1. pp. 457–462.

Fortin, D., Francus, P., Gebhardt, A.C., Hahn, A., Kliem, P., Lisé-Pronovost, A., et al.; PASADO Science Team. 2013. Destructive and non-destructive density determination: method comparison and evaluation from the Laguna Potrok Aike sedimentary record. Quaternary Science Reviews, **71**: 147–153. doi:10.1016/j.quascirev.2012.08.024.

Gagnon, A.S., and Gough, W.A. 2005. Trends in the dates of ice freeze-up and breakup over Hudson Bay, Canada. Arctic, **58**: 370–382. doi:10.14430/arctic451.

Gaye, B., Fahl, K., Kodina, L.A., Lahajnar, N., Nagel, B., Unger, D., and Gebhardt, A.C. 2007. Particulate matter fluxes in the southern and central Kara Sea compared to sediments: bulk fluxes, amino acids, stable carbon and nitrogen isotopes, sterols and fatty acids. Continental Shelf Research, **27**: 2570–2594. doi:10.1016/j.csr.2007.07.003.

Gearing, P., Plucker, F.E., and Parker, P.L. 1977. Organic carbon stable isotope ratios of continental margin sediments. Marine Chemistry, **5**: 251–266. doi:10.1016/0304-4203(77)90020-2.

Girard Thomas, M. 2009. Morphostratigraphie et evolution geomorphologique holocene du secteur sud du detroit de Nastapoka, est de la Baie d'Hudson. M.Sc. thesis, Universite Laval, Quebec, QC. 79 p. [In French.]

Gonthier, N., d'Anglejan, B., and Josenhans, H.W. 1993. Seismo-stratigraphy and sedimentology of Holocene sediments off Grande Rivière de la Baleine, southeastern Hudson Bay, Québec. Géographie Physique et Quaternaire, **47**: 147–166. doi:10.7202/032945ar.

Guo, L., Semiletov, I., Gustafsson, Ö., Ingri, J., Andersson, P., Dudarev, O., and White, D. 2004. Characterization of Siberian Arctic coastal sediments: implications for terrestrial organic carbon export. Global Biochemical Cycles, **18**: GB1036. doi:10.1029/2003GB002087.

Haberzettl, T., St-Onge, G., and Lajeunesse, P. 2010. Multi-proxy records of environmental changes in Hudson Bay and Strait since the final outburst flood of Lake Agassiz–Ojibway. Marine Geology, **271**: 93–105. doi:10.1016/j.margeo.2010.01.014.

Hare, A., Stern, G.A., Macdonald, R.W., Kuzyk, Z.Z., and Wang, F. 2008. Contemporary and preindustrial mass budgets of mercury in the Hudson Bay marine system: the role of sediment recycling. Science of the Total Environment, **406**: 190–204. doi:10.1016/j.scitotenv.2008.07.033. PMID:18765159.

Hill, P.R., Simard, A., and Héquette, A. 1999. High-resolution seismic stratigraphy of late Quaternary deposits in Manitounouk Sound, northern Quebec: effects of rapid post-glacial emergence. Canadian Journal of Earth Sciences, **36**(4): 549–563. doi:10.1139/e99-003.

Hudon, C., Morin, R., Bunch, J., and Harland, R. 1996. Carbon and nutrient output from the Great Whale River (Hudson Bay) and a comparison with other rivers around Quebec. Canadian Journal of Fisheries and Aquatic Sciences, **53**(7): 1513–1525. doi:10.1139/f96-080.

Hülse, P., and Bentley, S.J. 2012. A ^{210}Pb sediment budget and granulometric record of sediment fluxes in a subarctic deltaic system: the Great Whale River, Canada. Estuarine, Coastal and Shelf Science, **109**: 41–52. doi:10.1016/j.ecss.2012.05.019.

Jenner, K.A., and Piper, J.W. 2002. Grande Rivière de la Baleine, Hudson Bay, Québec — 1000 years of sedimentation. Geological Survey of Canada, Current Research, No. 2002-E10. 8 p. doi:10.4095/213691.

Jolivel, M. 2014. Érosion du pergélisol, transport fluvial et sédimentation marine, côte est de la baie d'Hudson, Nunavik, Canada. Ph.D. thesis, Université Laval, Québec, QC. 135 p. [In French.]

Jolivel, M., and Allard, M. 2013. Thermokarst and export of sediment and organic carbon in the Sheldrake River watershed, Nunavik, Canada. Journal of Geophysical Research, Earth Surface, **18**: 1–17. doi:10.1002/jgrf.20119.

Jones, P.D., New, M., Parker, D.E., Martin, S., and Rigor, I.G. 1999. Surface air temperature and its changes over the past 150 years. Reviews of Geophysics, **37**: 173–199. doi:10.1029/1999RG900002.

Josenhans, H.W., Balzer, S., Henderson, P., Nielson, E., Thorliefson, H., and Zevenhuisen, J. 1988. Preliminary seismostratigraphic and geomorphic interpretations of the quaternary sediments of Hudson Bay. *In* Current research, part B: Eastern and Atlantic Canada. Geological Survey of Canada, Paper 88-1B. pp. 271–286.

Kerwin, M.W., Overpeck, J.T., Webb, R.S., and Anderson, K.H. 2004. Pollen-based summer temperature reconstructions for the eastern Canadian boreal forest, subarctic, and Arctic. Quaternary Science Reviews, **23**: 1901–1924. doi:10.1016/j.quascirev.2004.03.013.

Klaminder, J., Appleby, P., Crook, P., and Renberg, I. 2012. Post-deposition diffusion of ^{137}Cs in lake sediment: implications for radiocaesium dating. Sedimentology, **59**: 2259–2267. doi:10.1111/j.1365-3091.2012.01343.x.

Kuzyk, Z.Z.A., Goñi, M.A., Stern, G.A., and Macdonald, R.W. 2008. Sources, pathways and sinks of particulate organic matter in Hudson Bay: evidence from lignin distributions. Marine Chemistry, **112**: 215–229. doi:10.1016/j.marchem.2008.08.001.

Kuzyk, Z.Z.A., Macdonald, R.W., Johannessen, S.C., Gobeil, C., and Stern, G.A. 2009. Towards a sediment and organic carbon budget for Hudson Bay. Marine Geology, **264**: 190–208. doi:10.1016/j.margeo.2009.05.006.

Kuzyk, Z.A.A., Macdonald, R.W., Tremblay, J.-E., and Stern, G.A. 2010. Elemental and stable isotopic constraints on river influence and patterns of nitrogen cycling and biological productivity in Hudson Bay. Continental Shelf Research, **30**: 163–176. doi:10.1016/j.csr.2009.10.014.

Ladouceur, S. 2008. Évaluation des changements environnementaux de la Baie d'Hudson et du Bassin de Foxe au cours des derniers siècles, à partir de traceurs palynologiques et micropaléontologiques. M.Sc. thesis, Université du Québec à Rimouski, Rimouski, QC. 79 p. [In French.]

Lajeunesse, P. 2008. Early Holocene deglaciation of the eastern coast of Hudson Bay. Geomorphology, **99**: 341–352. doi:10.1016/j.geomorph.2007.11.012.

Lajeunesse, P., and Allard, M. 2002. Sedimentology of an ice-contact glaciomarine fan complex, Nastapoka Hills, eastern Hudson Bay, northern Québec. Sedimentary Geology, **152**: 201–220. doi:10.1016/S0037-0738(02)00069-6.

Lajeunesse, P., and Allard, M. 2003. Late quaternary deglaciation, glaciomarine sedimentation and glacioisostatic recovery in the Rivière Nastapoka area, eastern Hudson Bay, Northern Québec. Géographie Physique et Quaternaire, **57**: 65–83. doi:10.7202/010331ar.

Lajeunesse, P., and St-Onge, G. 2008. The subglacial origin of the Lake Agassiz–Ojibway final outburst flood. Nature Geoscience, **1**: 184–188. doi:10.1038/ngeo130.

Laliberté, A.-C., and Payette, S. 2008. Primary succession of subarctic vegetation and soil on the fast-rising coast of eastern Hudson Bay, Canada. Journal of Biogeography, **35**: 1989–1999. doi:10.1111/j.1365-2699.2008.01932.x.

Lamb, A.L., Wilson, G.P., and Leng, M.J. 2006. A review of coastal palaeoclimate and relative sea-level reconstructions using δ^{13}C and C/N ratios in organic material. Earth-Science Reviews, **75**: 29–57. doi:10.1016/j.earscirev.2005.10.003.

Larouche, M.-E. 2010. Interaction entre la dégradation accélérée du pergélisol discontinu et l'organisation du réseau de drainage, Québec Subarctique. M.Sc. thesis, Université Laval, Québec, QC. 110 p. [In French.]

Lavoie, C., Allard, M., and Hill, P.R. 2002. Holocene deltaic sedimentation along an emerging coast: Nastapoka River delta, eastern Hudson Bay, Quebec. Canadian Journal of Earth Sciences, **39**(4): 505–518. doi:10.1139/e01-079.

Lavoie, C., Hill, P.R., Allard, M., St-Onge, G., and Lajeunesse, P. 2008. High-resolution seismo-stratigraphy and sedimentological properties of late- and postglacial sediments in Lac Guillaume-Delisle Estuary and Nastapoka Sound, eastern Hudson Bay. Canadian Journal of Earth Sciences, **45**(4): 427–441. doi:10.1139/E08-010.

Lavoie, C., Allard, M., and Duhamel, D. 2012. Deglaciation landforms and C-14 chronology of the Lac Guillaume-Delisle area, eastern Hudson Bay: a report on field evidence. Geomorphology, **159-160**: 142–155. doi:10.1016/j.geomorph.2012.03.015.

Liu, E., Yang, X., Shen, J., Dong, X., Zhang, E., and Wang, S. 2007. Environmental response to climate and human impact during the last 400 years in Taibai Lake catchment, middle reach of Yangtze River, China. Science of the Total Environment, **385**: 196–207. doi:10.1016/j.scitotenv.2007.06.041. PMID:17658584.

Marchildon, C. 2007. Évolution spatio-temporelle des palses et des lithalses de la région des rivières Sheldrake et Nastapoka, côte est de la baie d'Hudson, Nunavik, M.Sc. thesis, Département de Foresterie et Géomatique, Université Laval, Québec, QC. 101 p. [In French.]

McNeely, R., Dyke, A.S., and Southon, J.R. 2006. Canadian marine reservoir ages: preliminary data assessment. Geological Survey of Canada, Open file 5049. 3 p. doi:10.4095/221564.

Meyers, P.A. 1994. Preservation of elemental and isotopic source identification of sedimentary organic matter. Chemical Geology, **114**: 289–302. doi:10.1016/0009-2541(94)90059-0.

Meyers, P.A. 1997. Organic geochemical proxies of paleoceanographic, paleolimnologic, and paleoclimatic processes. Organic Geochemistry, **27**: 213–250. doi:10.1016/S0146-6380(97)00049-1.

Miltner, A., Emeis, K.-C., Struck, U., Leipe, T., and Voss, M. 2005. Terrigenous organic matter in Holocene sediments from the central Baltic Sea, NW Europe. Chemical Geology, **216**: 313–328. doi:10.1016/j.chemgeo.2004.11.016.

Mulder, T., Syvitski, J.P.M., Migeon, S., Faugères, J.-C., and Savoye, B. 2003. Marine hyperpycnal flows: initiation, behavior and related deposits. A review. Marine and Petroleum Geology, **20**: 861–882. doi:10.1016/j.marpetgeo.2003.01.003.

Muzuka, A.N.N., and Hillaire-Marcel, C. 1999. Burial rates of organic matter along the eastern Canadian margin and stable isotope constraints on its origin and diagenetic evolution. Marine Geology, **160**: 251–270 doi:10.1016/S0025-3227(99)00022-5.

Myers-Smith, I.H., Forbes, B.C., Wilmking, M., Hallinger, M., Lantz, T., Blok, D., et al. 2011. Shrub expansion in tundra ecosystems: dynamics, impacts and research priorities. Environmental Research Letters, **6**: 045509. doi:10.1088/1748-9326/6/4/045509.

Nagel, B., Gaye, B., Kodina, L.A., and Lahajnar, N. 2009. Stable carbon and nitrogen isotopes as indicators for organic matter sources in the Kara Sea. Marine Geology, **266**: 42–51. doi:10.1016/j.margeo.2009.07.010.

Naidu, A.S., Scalan, R.S., Feder, H.M., Goering, J.J., Hameedi, M.J., Parker, P.L., et al. 1993. Stable organic carbon isotopes in sediments of the north Bering-south Chukchi seas, Alaskan–Soviet Arctic Shelf. Continental Shelf Research, **13**: 669–691. doi:10.1016/0278-4343(93)90099-J.

Naidu, A.S., Cooper, L.W., Finney, B.P., Macdonald, R.W., Alexander, C., and Semiletov, I.P. 2000. Organic carbon isotope ratios ($\delta^{13}C$) of Arctic Amerasian Continental shelf sediments. International journal of Earth Sciences, **89**: 522–532. doi:10.1007/s005310000121.

O'Reilly, J., Leon Vintro, L., Mitchell, P.I., Donohue, I., Leira, M., Hobbs, W., and Irvine, K. 2010. 210Pb-dating of a lake sediment core from Lough Carra (Co. Mayo, western Ireland): use of paleolimnological data for chronology validation below the ^{210}Pb dating horizon. Journal of Environmental Radioactivity, **102**: 495–599. doi:10.1016/j.jenvrad.2010.09.003.

Orsi, T.H., Edwards, C.M., and Anderson, A.L. 1994. X-ray computed tomography: a non-destructive method for quantitative analysis of sediment cores. Journal of Sedimentary Research, Section A: Sedimentary Petrology and Processes, **64**: 690–693.

Oughton, D.H., Børretzen, P., Salbu, B., and Tronstad, E. 1997. Mobilisation of ^{137}Cs and ^{90}Sr from sediments: potential sources to arctic waters. The Science of the Total Environment, **202**: 155–165. doi:10.1016/S0048-9697(97)00112-5.

Payette, S., and Delwaide, A. 1991. Variations séculaires du niveau d'eau dans le bassin de la rivière Boniface (Québec nordique): une analyse dendroécologique. Géographie Physique et Quaternaire, **45**: 59–67. doi:10.7202/032845ar. [In French].

Payette, S., and Delwaide, A. 2000. Recent permafrost dynamics in a subarctic floodplain associated with changing water levels, Québec, Canada. Arctic, Antarctic and Alpine Research, **32**: 316–323. doi:10.2307/1552530.

Payette, S., and Filion, L. 1993. Holocene water-level fluctuations of a subarctic lake at the tree line in northern Québec. Boreas, **22**: 7–14. doi:10.1111/j.1502-3885.1993.tb00159.x.

Payette, S., Delwaide, A., Caccianiga, M., and Beauchemin, M. 2004. Accelerated thawing of subarctic peatland permafrost over the last 50 years. Geophysical Research Letters, **31**: 1–4. doi:10.1029/2004GL020358.

Payette, S., Filion, L., and Delwaide, A. 2008. Spatially explicit fire-climate history of the boreal forest-tundra (eastern Canada) over the last 2000 years. Philosophical Transactions of the Royal Society, **363**: 2301–2316. doi:10.1098/rstb.2007.2201. PMID:18048298.

Prinsenberg, S.J. 1986. The circulation pattern and current structure of Hudson Bay. *In* Canadian Inland Seas. *Edited by* Martini, I.P. Elsevier, New York. pp. 187–204.

Rachold, V., Grigoriev, M.N., Are, F.E., Solomon, S., Reimnitz, E., Kassens, H., and Antonow, M. 2000. Coastal erosion vs riverine sediment discharge in the Arctic Shelf seas. International Journal of Earth Sciences, **89**: 450–460. doi:10.1007/s005310000113.

Robbins, J.A., Edgington, D.N., and Kemp, A.L.W. 1978. Comparative ^{210}Pb, ^{137}Cs, and pollen geochronologies of sediments from Lakes Ontario and Erie. Quaternary Research, **10**: 256–278. doi:10.1016/0033-5894(78)90105-9.

Sampei, Y., and Matsumoto, E. 2001. C/N ratios in a sediment core from Nakaumi Lagoon, southwest Japan. Usefulness as an indicator. Geochemical Journal, **35**: 189–205. doi:10.2343/geochemj.35.189.

Saucier, F.J., Senneville, S., Prinseberg, S., Roy, F., Smith, G., Gachon, P., et al. 2004. Modelling the sea ice-ocean seasonal cycle in Hudson Bay, Foxe Basin and Hudson Strait, Canada. Climate Dynamics, **23**: 303–326. doi:10.1007/s00382-004-0445-6.

St-Onge, G., and Hillaire-Marcel, C. 2001. Isotopic constraints of sedimentary inputs and organic carbon burial rates in the Saguenay Fjord, Quebec. Marine Geology, **176**: 1–22. doi:10.1016/S0025-3227(01)00150-5.

St-Onge, G., and Long, B.F. 2009. CAT-scan analysis of sedimentary sequences: an ultrahigh-resolution paleoclimatic tool. Engineering Geology, **103**: 127–133. doi:10.1016/j.enggeo.2008.06.016.

St-Onge, G., Mulder, T., Francus, P., and Long, B. 2007. Chapter two continuous physical properties of cored marine sediments. *In* Proxies in Late Cenozic paleoceanography. Developments in Marine Geology, **1**: 63–98. doi:10.1016/S1572-5480(07)01007-X.

Stuiver, M., and Reimer, P.J. 1993. Extended (super 14) C data base and revised CALIB 3.0 (super 14) C age calibration program. Radiocarbon, **35**: 215–230.

Thornton, S.F., and McManus, J. 1994. Application of organic carbon and nitrogen stable isotope and C/N ratios as source indicators of organic matter provenance in estuarine systems: evidence from the Tay Estuary, Scotland. Estuarine, Coastal and Shelf Science, **38**: 219–233. doi:10.1006/ecss.1994.1015.

Tivy, A., Howell, S.E.L., Alt, B., McCourt, S., Chagnon, R., Crocker, G., et al. 2011. Trends and variability in summer sea ice cover in the Canadian Arctic based on the Canadian Ice Servie Digital Archive, 1960–2008 and 1968–2008. Journal of Geophysical Research, **116**: C03007. doi:10.1029/2009JC005855.

Voss, M., Deutsch, B., Elmgren, R., Humborg, C., Kuuppo, P., Pastuszak, M., et al. 2006. River biogeochemistry and source identification of nitrate by means of isotopic tracers in the Baltic Sea catchments. Biogeosciences Discussions, **3**: 475–511. doi:10.5194/bgd-3-475-2006.